Article:
Aleemardani, M. orcid.org/0000-0001-8261-4046, Johnson, L. orcid.org/0000-0001-7590-2154, Trikić, M.Z. et al. (2 more authors) (2023) Synthesis and characterisation of photocurable poly(glycerol sebacate)-co-poly(ethylene glycol) methacrylates. Materials Today Advances, 19. 100410. ISSN 2590-0498

https://doi.org/10.1016/j.mtadv.2023.100410

Materials Today Advances 19 (2023) 100410

Contents lists available at ScienceDirect

Materials Today Advances

journal homepage: www.journals.elsevier.com/materials-today-advances/

Synthesis and characterisation of photocurable poly(glycerol sebacate)-*co*-poly(ethylene glycol) methacrylates

Mina Aleemardani [a,b], Louis Johnson [a], Michael Zivojin Trikić [a], Nicola Helen Green [a,b], Frederik Claeyssens [a,b,*]

[a] Biomaterials and Tissue Engineering Group, Department of Materials Science and Engineering, Kroto Research Institute, The University of Sheffield, Sheffield, S3 7HQ, UK

[b] Insigneo Institute for in Silico Medicine, The Pam Liversidge Building, Sir Robert Hadfield Building, Mappin Street, Sheffield, S1 3JD, UK

ARTICLE INFO

Keywords:
Poly(glycerol sebacate)
Poly(glycerol sebacate)-*co*-poly(ethylene glycol)
Chemical modification
Methacrylation
Photocurable polymers

ABSTRACT

Poly (glycerol sebacate)-*co*-poly (ethylene glycol) (PGS-co-PEG) copolymers have multifunctional and tunable properties and great potential as high-performance biomaterials. However, the application of these materials is currently limited by harsh crosslinking conditions that include high temperatures and long reaction times. In this study, in order to overcome these limitations, the methacrylation process was conducted on PGS-co-PEG, resulting in photocurable (PGS-co-PEG)-M copolymers. Methacrylation of PGS-co-PEG, formulated respectively from polyethylene glycol (PEG2) or glycerol ethoxylate (PEG3), was investigated for the first time. (PGS-co-PEG2)-M and (PGS-co-PEG3)-M were found to be biodegradable, biocompatible, bioadhesive, pH-responsive and photocurable. Multifunctional characteristics remained after methacrylation, they were, however, drastically altered. Mechanical strength was enhanced significantly for (PGS-co-PEG)-M copolymers. Tensile Young's moduli of (PGS-co-PEG2)-M samples ranged from 0.08 to 0.48 MPa, while those of (PGS-co-PEG3)-M ranged from 2.67 to 35.47 MPa, indicating the mechanical properties of the materials can be tuned via crosslinking density. In contrast, bioadhesive properties, such as lap-shear and adhesion strengths, were almost halved due to methacrylation. The degradation and swelling rates were slightly reduced, but pH-responsive behaviours at pH = 5.0, 7.4 and 9.1 were still observed. Cell metabolic activity and double-stranded DNA content, investigated by resazurin and PicoGreen® assays, demonstrated that the (PGS-co-PEG)-M copolymers were biocompatible. Photocurable (PGS-co-PEG)-M copolymers facilitate a simple and user-friendly curing process (photo-crosslinking) that could be used for biomedical applications. Moreover, these photocurable copolymers are beneficial for various biofabrication methods, including emulsion techniques and additive manufacturing, either directly or indirectly.

1. Introduction

Poly (glycerol sebacate) (PGS) is one of several polymeric biomaterials that have been used recently in a variety of applications. The synthesis of PGS as a biodegradable polyester was outlined in 2002, and since then, because of its simple and reliable manufacture, it has gained popularity in tissue engineering. PGS synthesis involves polycondensation reactions between glycerol and sebacic acid, resulting in a 3D network of random coils with hydroxyl groups attached to the PGS backbone [1–3]. PGS is made of two natural components that can both be found in the body. Glycerol is the primary building block for lipids, whereas sebacic acid is a metabolic intermediate in the ω-oxidation of fatty acids [3–5]. These two precursors are also cheap and have Food and Drug Administration (FDA) approval [6]. PGS chemical and mechanical properties and degradation behaviour are determined by the synthesis parameters, which enable a tunable degree of esterification. Despite these benefits, PGS production and properties are not yet ideal for biological applications; for example, PGS production needs high curing temperatures, and PGS exhibits limited hydrophilicity. Indeed, unmodified or pure PGS crosslinks only in vacuum under high temperature ($\geq$120 °C) and long reaction times ($\geq$24 h) are required for thermal curing [4,7]. These harsh conditions mean complex 3D

* Corresponding author. Biomaterials and Tissue Engineering Group, Department of Materials Science and Engineering, Kroto Research Institute, The University of Sheffield, Sheffield S3 7HQ, UK.
E-mail address: F.Claeyssens@sheffield.ac.uk (F. Claeyssens).

https://doi.org/10.1016/j.mtadv.2023.100410
Received 12 May 2023; Received in revised form 11 July 2023; Accepted 21 July 2023
Available online 28 July 2023

architectures cannot be fabricated using simple manufacturing techniques. Moreover, these circumstances are not conducive to utilising the materials for purposes such as cell encapsulation. To address such drawbacks, PGS can be physically and chemically modified to improve its properties.

PGS is typically subjected to chemical modification(s) to change its chemical, mechanical, and degradation properties and to meet the needs of its intended use. In terms of crosslinking conditions, modified PGS is more adaptable without requiring further processing at high temperatures or in a vacuum, making it more appropriate for a range of applications [8,9]. For example, it was shown that diisocyanate, specifically hexamethylene diisocyanate (HDI), can effectively act as a crosslinker for PGS-based elastomers [10–13]. In a study conducted by Wang et al. a novel urethane-based PEGylated PGS (PEGS-U) bioelastomer was developed using HDI, which can be crosslinked at low temperatures. This crosslinking process led to the development of elastomers with highly-customised mechanical properties, hydrophilicity, and biodegradability [11]. Also, it was shown that by incorporating beta-tricalcium phosphate (β-TCP) powder in PEGS-U, rapid additive manufacturing at low temperatures is possible, and the printed grid scaffolds exhibited enhanced mechanical strength and hyperelasticity. These scaffolds supported cell proliferation and osteogenic differentiation and promoted new bone formation in critical-sized cranial defects [12]. PGS is most frequently chemically modified via acrylation [4,14] or methacrylation [8,15–17], particularly for additive manufacturing, stereolithography in particular. The presence of acrylate or methacrylate groups in PGS produces a photocurable PGS that can be photocrosslinked when combined with a free-radical generating photoinitiator and suitable wavelength of light (mainly UV light) [18,19], allowing it to be used in additive manufacturing techniques. PGS-based photocurable polymers can be crosslinked rapidly, almost within a few seconds up to a few minutes, which is one of their main advantages. Additionally, by simply changing the degree of acrylation or methacrylation, the characteristics of modified PGS can be altered [20,21].

Here, first, PGS was chemically modified by the addition of two types of polyethylene glycol (PEG), PEG2 (polyethylene glycol 1000) and PEG3 (glycerol ethoxylate 1000), as detailed in our previous study [22]. PEG is a polymer that is FDA approved, and when a PEG segment is added to the PGS backbone, a PGS-co-PEG copolymer is created that is less hydrophobic; therefore, it is more suited for biomedical applications [23,24]. Previously, we showed that adding PEG2 and PEG3 results in multifunctional copolymers with different characteristics, such as bioadhesion, flexibility, pH-responsive behaviour, degradability and cytocompatibility [22]. However, to cure PGS-co-PEG copolymers and make solid structures, harsh conditions (130 °C and 72 h in vacuum) were required. In this study, to address this issue, PGS-co-PEG copolymers, either PGS-*co*-PEG2 or PGS-*co*-PEG3, were methacrylated (developing (PGS-*co*-PEG)-M) in order to facilitate a simple and user-friendly curing process. To the best of our knowledge, this is the first study that synthesises and evaluates (PGS-co-PEG)-M copolymers, both (PGS-co--PEG2)-M and (PGS-co-PEG3)-M, with this methacrylation technique. (PGS-co-PEG)-M bioelastomers were characterised and showed multifunctional properties as before methacrylation but with noticeable alterations. Also, these photocurable copolymers can be used to make scaffolds with complex patterns such as micron-scale patterns and microparticles.

2. Materials and methods

2.1. Materials

Sebacic acid (SA), polyethylene glycol 1000 termed PEG2 (Mw = 1000 g/mol), glycerol ethoxylate termed PEG3 (Mw = 1000 g/mol), glycerol, tetrahydrofuran (THF), diphenyl(2,4,6-trimethylbenzoyl) phosphine oxide/2-hydroxy-2-methylpropiophenone (PI), Dulbecco's modified Eagle's medium (DMEM), amphotericin B, fetal bovine serum (FBS), penicillin/streptomycin (PS), L-glutamine, trypsin, paraformaldehyde, lipase, dimethyl sulfoxide (DMSO) and ethanol were all purchased from Sigma Aldrich.

2.2. Preparation of poly (glycerol sebacate)-co-poly (ethylene glycol) (PGS-co-PEG) copolymers

Following the method previously described by Aleemardani et al. the PGS-co-PEG copolymers, either PGS-*co*-PEG2 or PGS-*co*-PEG3, were synthesised [22]. Briefly, the copolymerisation of the PGS-*co*-PEG pre-polymer was carried out in two steps: (1) sebacic acid (SA) and PEG were polycondensed at various weight ratios to produce the SA/PEG pre-polymer, and (2) glycerol was added to the mixture to create the PGS-co-PEG pre-polymers. Two different PEG types, PEG 2-arm or PEG2 (Polyethylene glycol 1000; SIGMA, Mw = 1000 g/mol) and PEG 3-arm or PEG3 (Glycerol ethoxylated; SIGMA, Mw = 1000 g/mol), were employed in this study to synthesise the PGS-co-PEG prepolymers (Table 1). First, under stirring conditions, SA and PEG (20%, 40%, and 60% wt) were polycondensed. This was followed by a reaction at 130 °C with a nitrogen flow for 3 h and a vacuum of 9 mbar for 24 h. For PGS-co-PEG2 copolymers, PEG2 was first melted at 90 °C in a vacuum chamber. Second, glycerol was added and thoroughly mixed while under nitrogen flow, and the reaction was then carried out for 48 h at 130 °C and 9 mbar of vacuum (Fig. S1 Supporting Information).

2.3. Preparation of poly (glycerol sebacate)-co-poly (ethylene glycol) methacrylates (PGS-co-PEG)-M

The PGS-co-PEG copolymers were methacrylated in the following steps (Fig. 1A and B): The 100 g of PGS-co-PEG copolymers were dissolved in 400 ml of dichloromethane (Fisher Scientific, UK) for 1 h. Then 4-methoxyphenol was added at 1 mg/g of PGS-co-PEG prepolymer as a photo-polymerisation inhibitor due to the avoiding spontaneous crosslinking. Methacrylic anhydride (adding methacrylate groups) and triethylamine (as a neutralising base for the acidic side products like methacrylic acid) were added slowly. For PGS-co-PEG2, it was assumed that merely one hydroxyl group is available and others (two) reacted with sebacic acid. However, for PGS-co-PEG3, it was assumed that two hydroxyl groups are free, one hydroxyl group of glycerol and one hydroxyl group of glycerol ethoxylated. Therefore, the amounts of methacrylic anhydride and triethylamine for PGS-co-PEG3 were considered to be double compared to PGS-co-PEG2. The amounts of methacrylic anhydride (MEA) and triethylamine (TEA) are given in Table 1. The reaction temperature was 0 °C and after completion the mixture was allowed to equilibrate to room temperature over 24 h. Afterwards, further 4-methoxyphenol was then added at 0.5 mg/g of PGS-co-PEG prepolymer. Then the solution was washed three times with 30 mM hydrochloric acid (Fisher Scientific, UK) at 1:1 (v/v). Eventually, the solvent (dichloromethane) was removed by rotary evaporation under a vacuum pressure of 9 mbar to yield a viscous (PGS-co-PEG)-M prepolymer. The prepolymers were stored at −8 °C prior to use. Throughout this study, PGS-M with a degree of methacrylation (DM) of 80% was used as a control [15].

In order to make solid samples, 2% wt of photoinitiator (PI), diphenyl(2,4,6-trimethylbenzoyl) phosphine oxide/2-hydroxy-2-methylpropiophenone (Sigma Aldrich), was added into the (PGS-co-PEG)-M and PGS-M prepolymer solutions and were mixed. Then specimens were crosslinked by exposure to UV light (100 W, OmniCure Series 1000 curing lamp with an installed filter for 320–500 nm wavelengths) for 10 min (each side for 5 min). After photocrosslinking, all samples were washed with methanol (Fisher Scientific, UK) and PBS three times each to remove any residual of the solvent (dichloromethane). Samples were kept overnight in the oven at 60 °C to be dried prior to the experiments.

Table 1
Ratios of the PGS-co-PEG, both PEG 2-arm (PEG2) and 3-arm (PEG3), and the amounts of MEA and TEA used for methacrylation

Sample code		Molar ratio (PEG:Sebacic acid:Glycerol)	PEG (wt%)	MEA (g)	TEA (g)
PEG2	PEG3				
(PGS-co-20PEG2)-M	(PGS-co-20PEG3)-M	0.07:1:1	20	12.33 g for PGS-co-PEG2	8.10 g for PGS-co-PEG2
(PGS-co-40PEG2)-M	(PGS-co-40PEG3)-M	0.19:1:1	40	24.66 g for PGS-co-PEG3	16.20 g for PGS-co-PEG3
(PGS-co-60PEG2)-M	(PGS-co-60PEG3)-M	0.44:1:1	60		

2.4. Characterisation of (PGS-co-PEG)-M prepolymers by proton nuclear magnetic resonance (NMR) spectroscopy

To analyse PGS-M and (PGS-co-PEG)-M prepolymers, proton (^{1}H) nuclear magnetic resonance NMR spectroscopy (Burker AVIIIHD 400 NMR spectrometer) at 400 MHz was used. For recording standard ^{1}H experiments, a 30° pulse for excitation, 64 k acquisition points over a spectral (20.5 ppm width with 64 transients) and a 2s relaxation delay were utilised. Prepolymers were dissolved in deuterated chloroform ($CDCl_3$; 1 ml) at 1% w/v. $CDCl_3$ at 7.27 ppm was used as a standard for chemical shifts. MestReNova software was used to analyse spectra (MestreLab Research). To calculate the degree of methacrylation (DM), the signal integrals of the methylene groups in sebacic acid (1.3 ppm) and the methacrylate groups (1.9, 5.6, and 6.2 ppm) in each sample were used [15,16]. Among the samples, (PGS-co-40PEG3)-M showed a DM of 100%, so the DM of other specimens were reported in percentage by using the following Eq. (1) (Supporting Information):

$$\left(\int S\,I_{1.9} \Big/ \int S\,I_{1.3}\right) \Big/ \left(\int FMS\,I_{1.9} \Big/ \int FMS\,I_{1.3}\right) \times 100 \quad (1)$$

where S and FMS are sample and fully methacrylated sample ((PGS-co-40PEG3)-M), respectively.

2.5. Characterisation of (PGS-co-PEG)-M prepolymers by attenuated total reflectance-fourier transform infrared (ATR-FTIR)

Attenuated total reflectance-Fourier transform infrared (ATR-FTIR) spectroscopy was conducted on PGS-M and (PGS-co-PEG)-M samples before and after photocrosslinking by a Thermo Scientific Nicolet iS5 Fourier Transform Infrared (FTIR) with iD7 Single-Bounce ATR Accessories with readings between 400 and 4000 cm^{-1}, 4 cm^{-1} resolution, 16 scans.

2.6. Characterisation of (PGS-co-PEG)-M prepolymers using gel permeation chromatography (GPC)

The molecular weights of the prepolymer of PGS-M and (PGS-co-PEG)-M copolymers were determined using gel permeation chromatography (GPC) using Agilent 1260 Infinity with inbuilt refractive index detector. The samples were dissolved in THF (2 mg/ml) and then injected into the system at a constant flow rate of 1 ml/min. Polystyrene standards were utilised as a reference for calibration, and a toluene reference was incorporated (0.1% toluene was added to both samples/standards). Specimens were analysed at 35 °C by 2*x* PLgel 5 μm MIXED-C columns, 7.5 × 300 mm and a PLgel 5 μm column guard. The data analysis was performed using Agilent GPC/SEC Software (Version A.02.01 Build 9.3485). The chromatogram peaks were examined to determine the number average (M_n), weight average (M_w), and polydispersity index (DI) of the prepolymer molecular weights (Supporting Information).

2.7. Sol-gel content evaluation

A sol-gel content analysis was carried out on photocured PGS-M and (PGS-co-PEG)-M samples to define the degree of crosslinking. In this experiment, specimens (7 mm in diameter, 1.3 mm in thickness and n = 5) were weighed (W_0) and then allowed to swell in phosphate-buffered saline (PBS; 5 ml) and tetrahydrofuran (THF; 5 ml) for 48 h. The percentage of sol content was calculated by the following equation (Eq. (2)) after specimens had been thoroughly dried (W_d).

$$\text{Sol}\ (\%) = [(W_0 - W_d) / W_0] \times 100 \quad (2)$$

2.8. Swelling ratio (%) analysis

As part of this study, the specimens (n = 5; diameter: 0.7 cm; thickness: 1–1.2 mm) were weighed first (W_{dry}) before completely immersing in pH = 5.0 (citrate buffer; 1.5 ml), pH = 7.4 PBS (1.5 ml) and pH = 9.1 (glycine-NaOH buffer; 1.5 ml) and incubating at physiological temperature, 37 °C. After collecting the swollen samples at specific intervals, a filter paper was used to remove surface buffer and then the samples were weighed (W_{wet}). Swelling ratios were calculated using Eq. (3).

$$\text{Swelling ratio}\ (\%) = [(W_{wet} - W_{dry}) / W_{dry}] \times 100 \quad (3)$$

2.9. In vitro degradation test

The degradation kinetics of photocrosslinked (PGS-co-PEG)-M were studied over 35 days. To do so, firstly, the (PGS-co-PEG)-M samples (n = 5; diameter: 0.7 mm; thickness: 1.2–1.4 mm) were weighed (W_{ini}) and then incubated in the following degrading media: (1) PBS without enzymes (1.5 ml) and (2) PBS with lipase (110 U/L; 1.5 ml). In order to maintain full enzyme activity, the media was changed daily. The weight loss was determined at specific time intervals, 7, 14, 21, 28 and 35 days. At the end of the incubation period, the specimens were washed and dried, and then weighed (W_{day}). The following equation, Eq. (4), was used to calculate the weight loss (%).

$$\text{Weight loss}\ (\%) = [(W_{ini} - W_{day}) / W_{ini}] \times 100 \quad (4)$$

2.10. Poly (ethylene glycol) (PEG2) and glycerol ethoxylate (PEG3) release study

A two-phase colourimetric assay was used to quantify PEG release [25,26]. First, standard curves were obtained through serial dilution of a 20 mg/ml PEG2 and PEG3 stock solution in PBS. The reagent was prepared by dissolving 16.2 g of anhydrous ferric chloride ($FeCl_3$) in 1 L of distilled water and then adding 30.4 g of ammonium thiocyanate (NH_4SCN). In a microfuge tube, 0.5 ml of ammonium ferrothiocyanate reagent (upper phase) and chloroform (bottom phase) were added. The (PGS-co-PEG)-M and PGS-M (as a control) samples (7 mm in diameter and average of 1.4–1.9 mm thickness) were soaked in PBS at 37 °C. In a two-phase system microfuge tube, 50 μl aliquots of release media (PBS) from each sample were added at specific intervals for 35 days. At each interval, to keep the sink conditions constant over time, fresh PBS was replaced with constant withdrawn volume. A vortex and rocker were used to vigorously mix the tubes for 30 min, following which they were centrifuged at 5590 g for 2 min (Sanyo MSE Micro Centaur MSB010. CX2.5, UK). After removing the lower chloroform layers, the absorbance at 510 nm was measured with a UV spectrophotometer (JENWAY 6305). The replication of specimens was 5 (n = 5).

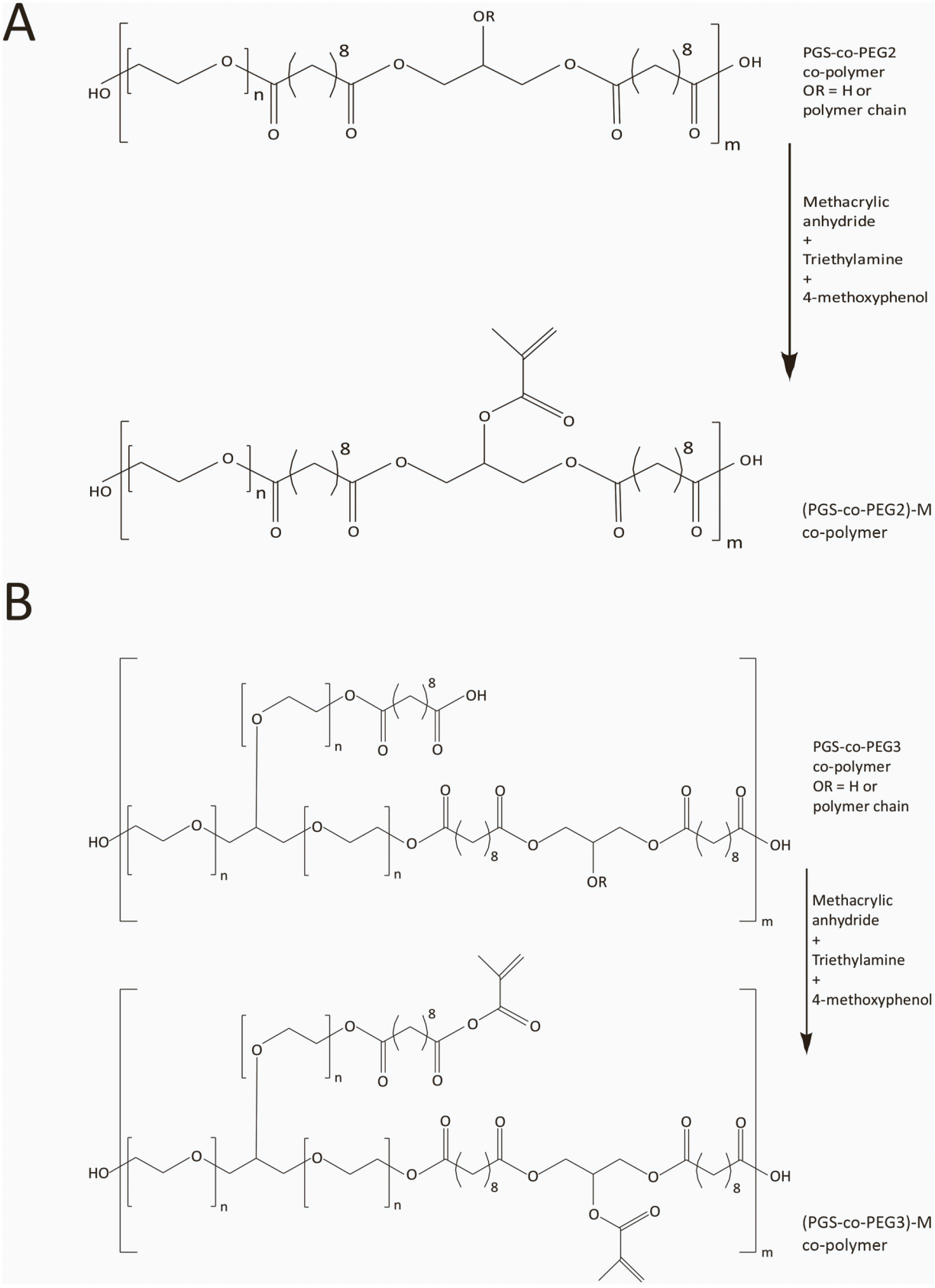

Fig. 1. Chemical structures of PGS-co-PEG2 and PGS-co-PEG3 after methacrylation, (A) (PGS-co-PEG2)-M and (B) (PGS-co-PEG3)-M, respectively.

2.11. Mechanical properties

2.11.1. Tensile test

Using a MultiTest-dV tester (Mecmesin, Slinfold, UK), the mechanical characteristics of (PGS-co-PEG)-M specimens were assessed following a modified version of ASTM D638-10. (PGS-co-PEG)-M solutions containing photoinitiator (PI) diphenyl(2,4,6-trimethylbenzoyl) phosphine oxide/2-hydroxy-2-methylpropiophenone (Sigma Aldrich) 2% wt (liquid phase) were injected into a dog-bone shaped PDMS mould in accordance with ASTM D638-10, and specimens crosslinked by exposure to UV light (100 W, OmniCure Series 1000 curing lamp) for 10 min (5 min for each side) (solid phase). With a load cell of 25 N, a grasp distance of 10 mm, and an extension rate of 1 mm/min, photocured samples were tested on a MultiTest-dV tester, and data on both force and elongation were collected. The linear-elastic area of each sample's stress-strain curve was used to compute tensile Young's modulus. The maximum elongation, also known as the elongation at yield, is the proportional elongation at the boundary of the linear elastic region, which was measured during the test. Each specimen had five replications (n = 5), and the samples ranged in thickness from 1 to 1.3 mm.

2.11.2. Compression test

Compressive properties of (PGS-co-PEG)-M samples with a dimension of 5 mm in diameter and 5 mm in height were measured. Dry (as-prepared) and swollen (hydrated, after 140 h being in PBS at 37 °C) samples were tested under compression using a MultiTest-dV tester (Mecmesin, Slinfold, UK) at a rate of 1 mm/min. Swollen samples were prepared to mimic the physiological conditions. For testing dry samples, a load cell of 15 N was employed, whereas a load cell of 5 N was utilised for testing wet samples. Due to the increased softness of the (PGS-co-PEG2)-M specimens, especially (PGS-co-60PEG2)-M after swelling, they were unable to withstand a 15 N load. At least five specimens were tested for each group, and the results were averaged. The data were obtained using Vector Pro software. Furthermore, to assess reversibility, the load was gradually released at the same rate, allowing for the acquisition of hysteresis diagrams for the specimens. The reversibility (after 10 s) was calculated from the height before loading (h_1) and after loading (h_2), Eq. (5) [27]:

$$\text{Reversibility}\ (\%) = [(h_2 - h_1)/h_1] \times 100 \quad (5)$$

The stress-strain curves were generated through a single loading-unloading cycle followed by 30 cyclic cycles. Cyclic load-unload cycles were tested in the same condition.

2.12. Lap-shear strength

A modified lap shear test based on the F2255-05 ASTM standard was used to quantify the shear strength of (PGS-co-PEG)-M samples in order to evaluate their bioadhesive characteristics [28]. Two pieces of glass slides with 10 mm × 50 mm dimensions were used, coated with a 20% w/v gelatin solution at 37 °C and dried at room temperature. Fifty milligrams of copolymers solution containing photoinitiator (PI) diphenyl(2,4,6-trimethylbenzoyl) phosphine oxide/2-hydroxy-2-methyl propiophenone (Sigma Aldrich) 2% wt were sandwiched between two overlayer glass slides and then crosslinked by exposure to UV light (100 W, OmniCure Series 1000 curing lamp) for 10 min (PGS-co-PEG)-M copolymers were cured between two glass slides by 10 mm × 10 mm dimensions. Shear strengths were measured at the detachment point of the samples (n = 5) by a MultiTest-dV tester (Mecmesin, Slinfold, UK) under tensile stress (1 mm/min). Dermabond™ Mini Topical Skin Adhesive was utilised as a control.

2.13. Wound closure test

A modified ASTM standard test, F2458-05, was performed on (PGS-co-PEG)-M specimens to evaluate wound closure capability [29,30]. This test was conducted using fresh porcine skin cut into pieces of 10 mm × 20 mm obtained from a local butcher shop. Before testing, the excess fat on the skin was removed and the remaining skin kept hydrated in PBS. To simulate a wound, a straight-edge razor was used to make an incision [31]. Super glue was used to attach the tissues to two glass slides (20 mm × 60 mm), resulting in about 10 mm of space was kept between the slides. Fifty milligrams of copolymers solution containing photoinitiator (PI) diphenyl(2,4,6-trimethylbenzoyl) phosphine oxide/2-hydroxy-2-methylpropiophenone 2% wt was administered onto the wound site and crosslinked by exposure to UV light (100 W, OmniCure Series 1000 curing lamp) for 10 min. The ultimate adhesive strength of (PGS-co-PEG)-M was calculated at the detachment point by a MultiTest-dV tester at a 1 mm/min strain rate (n = 5). As a control, Dermabond™ Mini Topical Skin Adhesive was used.

2.14. Adhesion test with different substrates and stainless steel calibration weights

The most adhesive sample, (PGS-co-60PEG2)-M, was used to adhere to different substances, including glass, polypropylene, polyethylene terephthalate, polytetrafluoroethylene, silicone, polystyrene, wood, stainless steel, and aluminium. Also, several stainless steel calibration weights were used to determine how much weight the sample could hold [22,32,33]. Typically, the joint was lightly compressed with a finger for 10 s before measuring the adhesion [22,33].

2.15. Cytocompatibility test

2.15.1. Preparing samples for cell culture and cell seeding

(PGS-co-PEG)-M and PGS-M samples (diameter of 10 mm) were washed in methanol and PBS and then dried. After that samples were sterilised with 70% ethanol (10 min, repeated three times), followed by a series of washes in sterile PBS (10 min, repeated three times). After sterilisation, the specimens ((PGS-co-PEG)-M and controls) were soaked overnight in foetal bovine serum (FBS) to improve the cell attachment. Immortalised human keratinocyte (HaCaT ATCC® HB-241TM) cells were maintained in adherent culture in a cell culture medium (DMEM containing 10% (v/v) FBS, 100 IU/ml penicillin, 100 mg/ml streptomycin, 2 mM L-glutamine and 0.625 μg/ml amphotericin B) at 37 °C and 5% CO_2. HaCaT cells were cultured and expanded in T75 flasks until they reached a confluent state of 70–80%. HaCaT cells were trypsinised and then seeded at a density of 2×10^4 (15 μl) cells per sample. Then samples were incubated for 30 min at 37 °C and 5% CO_2, and after that, 1 ml of medium was added. Tissue culture plastic (TCP) and PGS-M were used as controls. The medium was changed every two days during the culture of the cells for 1, 3 and 7 days. The replications of each sample were five (n = 5).

2.15.2. Evaluation of cell attachment, proliferation and viability

Cell attachment was evaluated on day 1, and cell proliferation and viability were measured on day 3 and day 7 using the resazurin reduction assay. A fluorescent plate reader can detect resorufin (fluorescent, pink), which has been reduced by the live cells from the resazurin solution (nonfluorescent, blue). A resazurin working solution was prepared by diluting a 1 mM resazurin stock solution with a cell culture media to 100 μM. In the following step, the scaffolds were transferred to a newly prepared well plate with sterile tweezers, and then a 1 ml solution of resazurin solution was added for each well. Well plates were incubated at 37 °C for 4 h with a foil cover to protect them from light. To read the related reductions, excitation and emission were measured at wavelengths of 540 nm and 630 nm, respectively, with a spectrofluorometer (FLX800, BIO-TEK Instruments, Inc.) by transferring duplicate samples of 200 μL of the reduced resazurin solution from each scaffold to a 96-well plate. Separate plates containing identical scaffolds were used to perform resazurin reduction assays at each interval (day 1, day 3 and day 7).

2.16. PicoGreen® assay

An alternative technique to investigate the growth and proliferation of HaCaT cells is to quantify double-stranded DNA (dsDNA) content at various time points. A PicoGreen assay is an established method to assess cell proliferation by quantifying dsDNA content. In this assay, the fluorescence intensity increases significantly when the PicoGreen dye intercalates with dsDNA molecules. The PicoGreen dye displays a low fluorescence when it is free in solution; however, once it binds to dsDNA, it experiences a change in its fluorescence emission spectrum, producing a higher signal that can be detected with a fluorescence plate reader.

The DNA content was measured using a Quant-iT™ PicoGreen® dsDNA Kit. Seeded HaCaT cells on (PGS-co-PEG)-M and PGS-M samples with a diameter of 10 mm were transferred into 24-well plates on day 3 and day 7. Cell digestion or lysing buffer (1 ml containing 10 mM Tris-HCl, 1 mM $ZnCl_2$ and 1% Triton-X100 in distilled water (dH_2O)) was added to the specimens and incubated for 30 min at room temperature. Then samples were vortexed for 60 s and kept overnight in a fridge at 4 °C. The (PGS-co-PEG)-M samples and controls (PGS-M and TCP) then underwent 3 *x* freeze-thaw cycles (10 min at - 80 °C and 20 min at 37 °C, 15 s vortex between the freeze-thaw cycles). To make the PicoGreen working solution, 20 × Tris-EDTA (TE) was diluted 1:20 in dH_2O (1:TE), and the PicoGreen reagent was diluted 1:200 in 1 × TE. 100 μL PicoGreen working solution was mixed with 100 μL of the lysate of samples (1:1 v/v) in 96-well plates wrapped in foil and incubated at room temperature for 10 min. Excitation wavelength was 485 nm, and emission wavelength was 528 nm during fluorescence measurements (FLX800, BIO-TEK Instruments, Inc.). For each sample, an approximate number of cells on day 3 and day 7 was calculated using the standard curve generated from the relative fluorescence of PicoGreen of HaCaT cells at 10,000, 25,000, 50,000, 100,000 and 150,000 cell counts.

2.17. Immunofluorescence staining

On day 3, (PGS-co-PEG)-M and PGS-M were fixed with 3.7% formaldehyde (FA) for 20 min and washed gently with PBS before submerging into 0.1% (v/v) Triton X 100 (in PBS) for 20 min. After three times PBS washing, to visualise F-actin filaments in cells, phalloidin (FITC, Sigma Aldrich) solution was added (1:500 diluted in PBS from stock solution) to samples and incubated for 30 min in the dark. Samples were washed three times with PBS. The nuclei of the cells were stained with 4′,6-diamidino-2-phenylindole (DAPI, Sigma Aldrich) solution (diluted 1:1000 in PBS) and incubated in the dark for 15 min; samples were then washed three times with PBS and imaged with an LSM880 AiryScan Confocal Microscope (ZEISS, Germany) with equipped with using a 10*x*/0.3 Plan-Neofluar objective. DAPI images were excited using a 405 nm laser and spectrally detected in the 410–495 nm range. The FITC (green) channel was imaged with 488 nm laser excitation and spectral detection of 495–634 nm. Z-stack images (2580 × 2580 pixels) were taken for each sample and projected to a single image.

2.18. Statistical analysis

The results were analysed using Origin Pro 2020 and one-way and two-way analysis (for resazurin and PicoGreen results; mentioned within the text) of variance (ANOVA). Tukey (one-way) and Bonferroni (two-way) analyses were used, and results were plotted as mean ± standard deviation (SD). The p-values in the figures show the statistical differences between the groups (*P < 0.05, **P < 0.01 and ***P < 0.001). The Materials and methods section and the figure legends both mention the number of replicates (n).

3. Results and discussion

3.1. Proton (^1H) nuclear magnetic resonance (NMR) spectroscopy

A ^1H NMR analysis demonstrated that PGS-M and (PGS-co-PEG)-M, either (PGS-co-PEG2)-M or (PGS-co-PEG3)-M, were successfully synthesised (Fig. 2A, B and 2C). Spectra of sebacic acid $–COCH_2CH_2CH_2-$ were confirmed at 2.3, 1.6, and 1.3 ppm (c, d and e); and of glycerol $–CH_2CH–$ with peaks at 5.2, 4.2, 3.7 ppm (a and b). The signals of the methacrylate groups peaked at 6.2, 5.6 and 1.9 ppm (g). Due to the use of DCM in the methacrylation process, residual DCM was found even after rotary evaporation - peaks at 5.3 ppm were associated with DCM [15]. As a result of the inclusion of the PEG, the methylene peaks showed up (f) in the spectra of (PGS-co-20PEG2)-M (at 3.67 ppm), (PGS-co-40PEG2)-M (at 3.66 ppm), (PGS-co-60PEG2)-M (at 3.69 ppm), (PGS-co-20PEG3)-M (at 3.65 ppm), (PGS-co-40PEG3)-M (at 3.68 ppm) and (PGS-co-60PEG3)-M (at 3.67 ppm) [22,24,34,35]. The degree of methacrylation for (PGS-co-PEG)-M samples was calculated using Eq. (1), and (PGS-co-PEG2)-M and (PGS-co-PEG3)-M had the DM of almost 10–43% and 70–100%, respectively (Table S1 Supporting Information). Also, the actual percentages of PEG obtained from ^1H NMR analysis closely matched the theoretical PEG percentages, indicating a properly controlled copolymer synthesis (Table S1 Supporting Information).

3.2. Attenuated total reflectance-fourier transform infrared (ATR-FTIR)

ATR-FTIR spectra of PGS-M and (PGS-co-PEG)-M samples before (liquid) and after (solid) photocuring are given in Fig. 2D, E and 2F. For PGS-M, broad peaks associated with hydroxyl groups were found around 3468 cm^{-1}, and two strong peaks were present at 2922 cm^{-1} and 2854 cm^{-1} associated with methyl and alkane groups. A sharp peak at 1734 cm^{-1} was seen related to ester bonds, and the peaks between 1292 and 1048 cm^{-1} were associated with carboxyl stretch vibrations. Distinct peaks related to the methacrylate groups were observed at 946 cm^{-1} (=C–H bending) and 1642 cm^{-1} (C]C stretching). These peaks were reduced significantly or even removed after UV photopolymerisation (Fig. 2D) [8,15,36]. For (PGS-co-PEG)-M copolymers compared with the PGS-M, a band around 1120 cm^{-1} (C–O–C) was observed related to symmetric stretching vibrations [22,37]. Also, other peaks about 1150–1170 cm^{-1} were associated with the ether bonds in (PGS-co--PEG)-M samples, resulting in a successful segmentation of the backbone of the PGS-co-PEG [22]. After UV photopolymerisation, some changes for peaks labelled by a, b, c, d, e and f were observed (Fig. 2D, E and 2F). Sharp peaks attributed to hydroxyl groups (O–H stretching labelled by a) were observed around 3600–3500 cm^{-1} [38], but after photocrosslinking, these peaks strongly reduced in intensity. The reduction in intensity is potentially related to the consumption of the hydroxyl end-groups during the formation of ester crosslinking with the methacrylate groups [39]. Asymmetric and symmetric stretching vibrations of C–H bonds (peaks labelled by b) were detected at around 2980 and 2880 cm^{-1}, respectively, but after photocrosslinking, these peaks were shifted to 2928 and 2861 cm^{-1}, respectively. The shift and reduction in intensity of C–H vibrations after crosslinking indicates the conversion of methacrylate alkene groups to alkane groups. Additionally, the intensity of the peaks decreased after crosslinking. Carbon dioxide peaks were detected around 2300–2400 cm^{-1} (labelled by c), resulting from measuring conditions. After photocuring, the intensity of these peaks reduced noticeably, which could be related to CO_2 permeability (gas permeability is higher in liquids) [40]. Ester bonds (labelled by d) within the (PGS-co-PEG)-M copolymers were demonstrated by firm peaks roughly at 1733 cm^{-1} (C]O), which were intensified after photocrosslinking under UV light. However, the methacrylate peaks at around

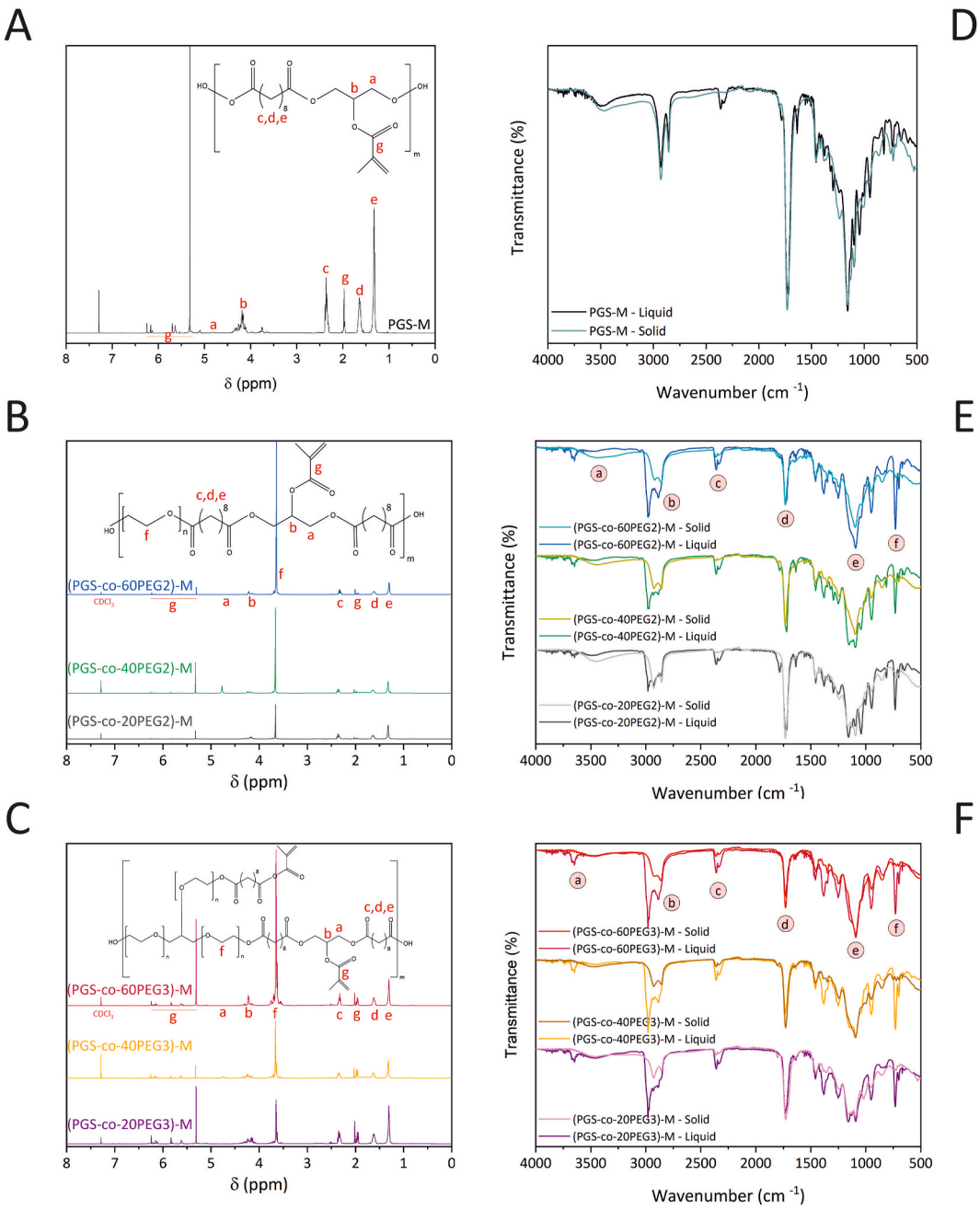

Fig. 2. ^{1}H NMR spectra of (A) PGS-M polymer, (B) (PGS-*co*-PEG2)-M copolymers and (C) (PGS-*co*-PEG3)-M copolymers. The ATR-FTIR spectra of (D) PGS-M polymers, (E) (PGS-*co*-PEG2)-M copolymers and (F) (PGS-*co*-PEG3)-M copolymers were obtained before and after the photocrosslinking process.

740–750 cm^{-1} (labelled by f), 945 cm^{-1} (peaks in the area of label e) and 1644 cm^{-1} decreased after photocuring [8]. Some of the groups consumed after photocrosslinking, such as C]C bonds, become C–C or C] O bonds, and their intensity changes accordingly [41].

3.3. Characterisation of (PGS-co-PEG)-M prepolymers using gel permeation chromatography (GPC)

GPC was conducted on (PGS-co-PEG)-M and PGS-M to determine the effect of methacrylation on the number and weight averaged molecular

Table 2
GPC results of (PGS-co-PEG2)-M and (PGS-co-PEG3)-M copolymers, including the number average (M_n), weight average (M_w), and polydispersity index (DI) (Supporting Information).

Sample	*M_n (g/mol)*	*M_w (g/mol)*	*DI*	*Sample*	*M_n (g/mol)*	*M_w (g/mol)*	*DI*
(PGS-co-20PEG2)-M	2755	7313	2.654	(PGS-co-20PEG3)-M	3508	20398	5.815
(PGS-co-40PEG2)-M	2625	5373	2.047	(PGS-co-40PEG3)-M	3562	17504	4.914
(PGS-co-60PEG2)-M	2392	4494	1.879	(PGS-co-60PEG3)-M	3466	10234	2.953

weights and dispersity index (M_n, M_w and DI). The M_w of PGS-M was determined to be 11007 g/mol, with an M_n of 2547 g/mol and a DI of 4.322. As indicated in Table 2 (Supporting Information), there was an observed increase in molecular weight (Mw) following the methacrylation process, indicating that the reaction led to the incorporation of methacrylate functional groups into the polymer chains. The extent of the molecular weight increase varies depending on various factors, such as the extent of conversion of methacrylate functional groups, the reaction efficiency, and the initial molecular weight of the polymer. Comparing the molecular weight before [22] and after methacrylation, show that the molecular weights of (PGS-co-PEG)-M and PGS-M increase upon methacrylation. This increase can be related to methacrylate groups attached to the polymer chains, adding mass to the polymer structure.

3.4. Sol-gel content

To investigate the crosslinking density, the sol-gel content assay can be used. In theory, the crosslinked parts swell in the THF solution while the non-crosslinked segments leach out. Hence, the sol and gel content can be calculated based on the remaining dry weight of the crosslinked network [42]. Here, sol content (%) was measured in both PBS and THF for a better comparison. PBS was used to examine the sol content in a similar condition to the biological environment. THF was utilised because it is a common solvent to evaluate the sol-gel content since the swelling degree of co/polymers is high, which allows the sol to diffuse out. Previous studies indicated that the sol content increases with the addition of PEG because of lower crosslinking density [22,37,43], and the results given in Fig. 3A are consistent with the expected trend. In our former study, we have shown that adding PEG reduces the percentage of gel content, but this decrease depends on both concentration and type of PEG [22]. As can be seen in Fig. 3A, loading PEG indeed enhanced the sol (%), and higher concentrations of PEG led to greater percentages of sol; however, the amounts of sol content (%) of (PGS-co-PEG2)-M were remarkably higher than (PGS-co-PEG3)-M ($P < 0.001$). Although similar trends were seen in our previous research [22], here, the gaps in sol values between (PGS-co-PEG2)-M and (PGS-co-PEG3)-M were more significant. For instance, the sol content (%) of (PGS-co-60PEG2)-M and (PGS-co-60PEG3)-M were 50.35 ± 5.19% and 18.07 ± 1.06%, respectively in THF. Due to the structure of PEG3 (having 3-arm rather than 2-arm), after methacrylation, based on the obtained results, such as swelling, in vitro degradation and sol-gel content, it can be concluded that (PGS-co-PEG3)-M has higher crosslinking density than (PGS-co--PEG2)-M. Also, by comparing the results between the present and previous study, we can conclude that the crosslinking densities of (PGS-co-PEG3)-M are higher than non-methacrylates PGS-co-PEG3 copolymers that were thermally crosslinked [22]. The presence of free hydroxyl groups (-OH groups) on the polymer backbone is related to the formation of covalent crosslinks. A higher abundance of free –OH groups can be found in PGS-co-PEG3 than in PGS-co-PEG2, and due to this, there are more methacrylic groups in (PGS-co-PEG3)-M than (PGS-co--PEG2)-M. Therefore, the changes in sol content were much lower in (PGS-co-PEG3)-M than in (PGS-co-PEG2)-M.

3.5. Swelling ratio (%) analysis

3.5.1. Swelling in pH = 7.4

In order to measure the bulk hydration characteristics of PGS-M polymer and (PGS-*co*-PEG)-M copolymers, swelling ratios (%) at pH = 7.4 were calculated [44] (Fig. 3E). The swelling capacity is typically governed by hydrophilicity, interactions between polymers, and crosslink density [45]. In all (PGS-co-PEG3)-M copolymers, water uptake and

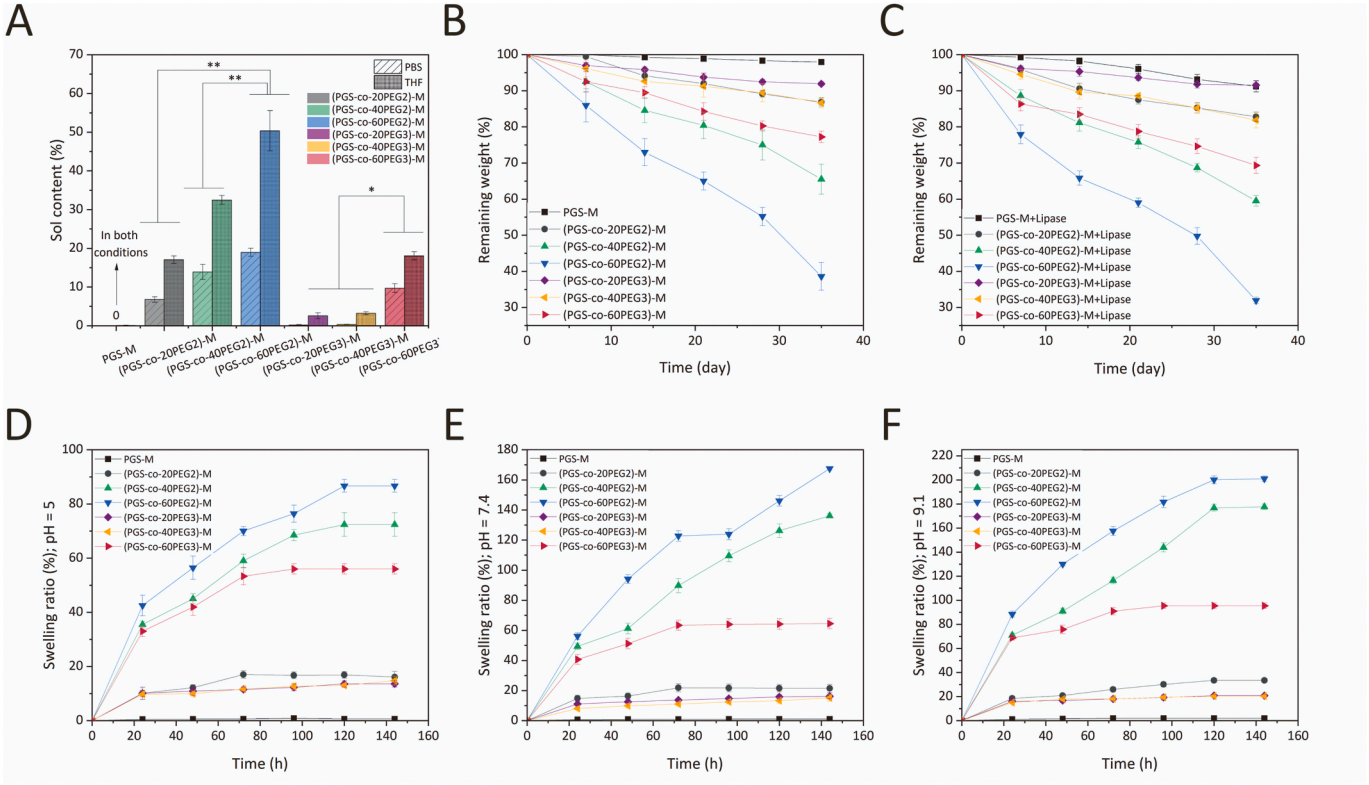

Fig. 3. (A) Sol content (%) of PGS-M and (PGS-co-PEG)-M samples within PBS and THF after 48 h. PGS-M was the control in this test, and its sol content was 0 ± 0% in PBS and 0.06 ± 0.08% in THF after 48 h (* p-value <0.05 and ** p-value <0.01). In vitro degradation curves of (B) the (PGS-co-PEG)-M samples in (B) PBS and (C) PBS with lipase (110 U/L) for 35 days (n = 5). pH-responsive water swelling ratios of PGS-M and (PGS-co-PEG)-M samples were measured at (D) pH 5.0, (E) pH 7.4, and (F) pH 9.1 over 144 h (n = 5).

equilibrium water content were achieved within 72 h, whereas the (PGS-co-40PEG2)-M and (PGS-co-60PEG2)-M equilibrated after 144 h, reaching 136.15 ± 1.50% and 167.49 ± 0.89%, respectively, which were the maximum percentages. As the amount of PEG2 and PEG3 increased, swelling enhanced significantly, but the swelling ratios of (PGS-co-PEG2)-M were higher than (PGS-co-PEG3)-M. This difference could be related to the lower crosslinking density and lower molecular weight of (PGS-coPEG2)M specimens [22]. The water swelling ratio for pure PGS-M was 1.01 ± 0.33%, but adding either PEG2 or PEG3 enhanced this ratio substantially. Addition of PEG to PGS results in an increase in hydrophilicity that is directly proportional to its concentration [22,24,36,46]. In addition, (PGS-co-PEG)-M copolymers could be considered hydrogels due to their high swelling ratios.

3.5.2. pH-responsive behaviours (swelling in pH = 5.0 and 9.1)

A variety of pH ranges are found within the human body due to physiological functions and medical conditions [47]. pH regulation is fundamental for maintaining a healthy equilibrium in biological environments. Biological systems can experience changes in pH as a result of disturbances and dysfunctions. Hence, being able to detect pH changes in a biological context could be of great benefit [48]. In many biomedical and tissue engineering applications, hydrogels or hydrophilic polymers with pH-responsive properties have great potential to act as sensors of pH since these biomaterials can adapt based on environmental pH levels [49]. In (PGS-co-PEG)-M, mostly hydroxyl groups and carboxyl groups formed covalent crosslinks; however, some ionic functional groups can be retained in copolymer hydrogels. Mainly, the carboxyl (–COOH) can be ionised by deprotonation, becoming negatively charged carboxyl ($–COO^-$) [22]. Therefore, to explore the pH responsiveness of (PGS-co-PEG)-M copolymers, swelling assays over 144 h at three different pH levels, 5.0, 7.4 and 9.1 were performed. At acidic (citrate buffer, pH 5.0) and basic (NaOH-glycine buffer, pH 9.1) pH, the PBS swelling ratio of (PGS-co-PEG)-M samples is displayed in Fig. 3D–F. There was more swelling in alkaline than in neutral or acidic conditions for (PGS-co-PEG2)-M and (PGS-co-PEG3)-M (Fig. 3F). However, the swelling ratio was lowest in acidic environments (Fig. 3D). The swelling ratios (%) of (PGS-co-PEG3)-M reached their equilibrium after 72 h at pH 5.0. The swelling of (PGS-co-20PEG3)-M was 11.52 ± 0.82%, (PGS-co-40PEG3)-M was 11.70 ± 0.85% and (PGS-co-60PEG3)-M was 53.31 ± 3.15%, while (PGS-co-PEG2)-M remained at equilibrium after 120 h. The swelling of (PGS-co-20PEG2)-M was 16.90 ± 1.23%, (PGS-co-40PEG2)-M was 72.45 ± 4.37% and (PGS-co-60PEG2)-M was 86.67 ± 2.36%. In contrast, swelling ratios increased significantly for samples at pH 9.1, reaching equilibrium at 120 h, to 33.52 ± 1.81% for (PGS-co-20PEG2)-M, 176.79 ± 2.85% for (PGS-co-40PEG2)-M, 200.08 ± 3.19 for (PGS-co-60PEG2)-M, 20.82 ± 1.01% for (PGS-co-20-PEG3)-M, 20.45 ± 0.65% for (PGS-co-40PEG3)-M and 95.45 ± 2.40% for (PEG-co-60PEG3)-M. The water swelling equilibria were reached for (PGS-co-PEG3)-M at pH 5.0 and pH 7.4 after 72 h, but at pH 9.1 the equilibrium was reached after 120 h; whereas (PGS-co-PEG2)-M reached their equilibrium after 120 h at all three conditions. (PGS-co-40PEG2)-M and (PGS-co-60PEG2)-M showed significantly higher swelling ratios at pH 9.1 than the other samples (Fig. 3D–F). The ionisation of carboxyl groups is much easier when hydrophilic segments of the amphiphilic structure are dominant, such as in (PGS-co-PEG)-M [22,50,51]. It is also important to have free space and more chain relaxation to ionise carboxyl groups [22,23,50,51], which (PGS-co-PEG3)-M copolymers, due to their higher crosslinking density, are less likely to provide. As a result, (PGS-co-40PEG2)-M and (PGS-co-60PEG2)-M were more hydrophilic than other samples. It is worth mentioning that generally, PGS-based polyesters are easier to degrade in a basic (alkaline) solution compared to an acidic solution. Yoon et al. [46] observed that similar PGS-gelatine-based hydrogels under acidic conditions are less prone to swell; this is also indicated by our previous study on non-methacrylated PGS-co-PEG [22], and the swelling behaviour of the methacrylated PGS-co-PEG formulations, (PGS-co-PEG)-M, presented in this study. This is likely because the protonation of free carboxylic acid groups within the PGS-co-PEG renders the material more hydrophobic, hence less prone to water ingress and subsequent hydrolytic degradation.

3.6. In vitro degradation test

An in vitro study of (PGS-co-PEG)-M degradation kinetics was conducted over 35 days. In both PBS with and without lipase, degradation profiles can be observed because ester bonds were hydrolysed; however, degradation was accelerated when lipase was present [52] (Fig. 3B–C). The degradation profiles show that in vitro degradation rates are directly related to the amount of PEG incorporation [22]. As a result of 35 days in PBS, (PGS-co-40PEG2)-M and (PGS-co-60PEG2)-M samples lost the greatest amounts of weight, with the remaining weights of 65.51 ± 4.15% and 38.61 ± 3.83%, respectively. In the presence of lipase in the degradation media, all the degradation rates were higher, but again (PGS-co-40PEG2)-M and (PGS-co-60PEG2)-M had the greatest loss, and the remaining weights were 59.53 ± 1.49% and 31.94 ± 0.92%, respectively. Previously, these two samples had better hydration as measured by water swelling ratios, which could lead to greater degradation. It can be concluded that higher PEG concentrations cause higher swelling ratios, and this can result in faster degradation rates due to the higher hydrophilicity [11]. These results are consistent with the trends observed for PGS-co-PEG2 and PGS-co-PEG3 in the previous study [22]. It was generally found that (PGS-co-PEG2)-M had higher degradation ratios than (PGS-co-PEG3)-M, which can be related to the lower crosslinking density of (PGS-co-PEG2)-M.

3.7. Poly (ethylene glycol) (PEG2) and glycerol ethoxylate (PEG3) release study

To evaluate the crosslinking density of samples a PEG release assay was also conducted. This test is a colourimetric assay using a two-phase system; based on the observation that whenever ferrothiocyanate-PEG complexes are made in the chloroform phase, a visible purple-pink colouration can be observed, which is detectable at a wavelength of 510 nm [22,25]. All the (PGS-co-PEG)-M samples had PEG releases into media, and those specimens that contained higher percentages of PEG, released greater amounts of PEG. However, the (PGS-co-PEG2)-M copolymers had remarkably higher PEG release than (PGS-*co*-PEG3)-M ($P < 0.001$) (Fig. 4). On day 35, the PEG release (%) of (PGS-co-20PEG2)-M was 1.33 ± 0.19%, (PGS-co-40PEG2)-M was 5.73 ± 0.31%,

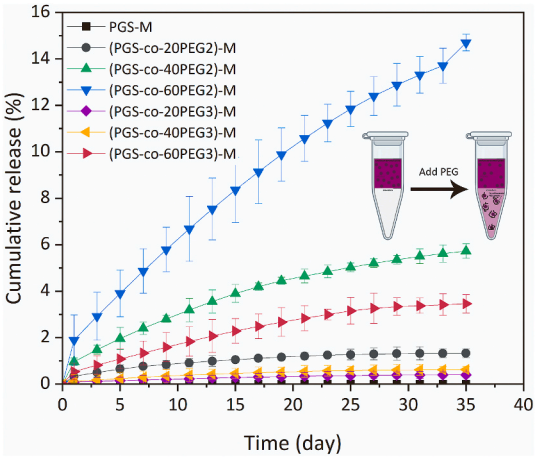

Fig. 4. Results of cumulative PEG release (%) of (PGS-co-20PEG2)-M, (PGS-co-40PEG2)-M, (PGS-co-60PEG2)-M, (PGS-co-20PEG3)-M, (PGS-co-40PEG3)-M and (PGS-co-60PEG3)-M samples and control (PGS-M) for 35 days (n = 5). During the whole 35 days of the PEG release study, there was no release of PEG for a control group, PGS-M.

(PGS-co-60PEG2)-M was 14.70 ± 0.36%, (PGS-co-20PEG3)-M was 0.40 ± 0.11%, (PGS-co-40PEG3)-M was 0.63 ± 0.13% and (PGS-co-60-PEG3)-M was 3.46 ± 0.39%. Therefore, as we previously have shown [22], both concentration and type of PEG affect the PEG release. Higher percentages of PEG lead to higher amounts of released PEG, and PEG2 has significantly higher PEG release than PEG3. The highest PEG release among (PGS-co-PEG2)-M was for (PGS-co-60PEG2)-M around ~15%, while the maximum release of PEG in (PGS-co-PEG3)-M samples was for (PGS-co-60PEG3)-M, reaching ~3.5% (Fig. 4). In general, (PGS-co--PEG2)-M had greater PEG release than (PGS-co-PEG3)-M as well as higher sol content, more swelling and faster in vitro degradation, which could be related to the higher crosslinking density of (PGS-co-PEG3)-M. Furthermore, the PEG release profiles of (PGS-co-PEG3)-M were noticeably lower than PGS-co-PEG3, which can conclude that methacrylated samples had higher crosslinking densities than the non-methacrylated thermally cured specimens.

3.8. Mechanical properties

As demonstrated in our previous study, adding PEG, either PEG2 or PEG3, to the PGS backbone considerably improved the elastomeric properties, showing that PGS-co-PEG can withstand extreme deformations without fragmentation. As a result of adding PEG2 to PGS, materials were softer, more flexible, and less strong than those made with PEG3, which is related to crosslinking density [22]. Here, both tensile and compression tests were conducted to evaluate the changes in mechanical behaviour after methacrylation. Generally, after methacrylation, all the samples, PGS-M, (PGS-co-PEG2)-M and (PGS-co--PEG3)-M, had significantly higher mechanical strength than non-methacrylated ones ($P < 0.01$).

3.8.1. Tensile test

Tensile Young's moduli of (PGS-co-PEG3)-M were remarkably higher than (PGS-co-PEG2)-M ($P < 0.001$), which is likely related to the higher number of methacrylic groups in (PGS-co-PEG3)-M as initially for the functionalisation (methacrylation) more free –OH groups (functional groups) were considered. In addition, according to NMR results (Fig. 2A-C), (PGS-co-PEG3)-M had higher degrees of methacrylation than (PGS-co-PEG2)-M. A high degree of methacrylation results in a higher crosslinking density, which in turn results in greater mechanical strength [8,20]. As PEG concentration increased, tensile Young's moduli for both (PGS-co-PEG2)-M and (PGS-co-PEG3)-M decreased (Fig. 5B). Soft chain segments are introduced into the copolymer structure by PEG, and higher concentrations of PEG reduce rigid chain segments in PGS. Moreover, the presence of PEG lowers the esterification level and finally results in prepolymers with lower molecular weights; therefore, higher amounts of PEG lead to lower tensile Young's modulus [22,35,37]. Although the addition of PEG decreased mechanical strength (tensile Young's modulus), it increased maximum elongation, which enhanced flexibility (Fig. 5C).

3.8.2. Compression test

Obtained load-unload compressive stress-strain curves (Fig. 5D–G) indicated that (PGS-co-PEG2)-M samples were much softer than (PGS-co-PEG3)-M in both dry and swollen conditions. The stress-strain curves of (PGS-co-PEG3)-M (stiff materials) exhibited an abrupt initial increase, indicating a strong resistance to deformation, whereas (PGS-co-PEG2)-M (soft materials) demonstrated a lower initial stiffness with a more gradual gradient. Also, (PGS-co-PEG3)-M only showed to have elastic behaviour, which aligns with the characteristics of stiff and tough polymers. Stiff polymers may not have a distinct yield point and tend to deform elastically until they reach their ultimate strength, displaying minimal or negligible plastic deformation (Video 4 Supporting Information). From the compressive stress-strain curves, it is evident that the mechanical strength of the swollen samples slightly decreased compared to the dry specimens. This decrease was highly noticeable in (PGS-co-60PEG2)-M, which reduced the compressive Young's modulus from 0.33 ± 0.15 to 0.04 ± 0.02 MPa ($p < 0.001$) (Fig. 5F–H).

To show the abilities of (PGS-co-PEG)-M samples for reversible deformations, 30 cyclic compression tests were conducted in both dry (as-prepared) and swollen (hydrated) conditions. All the samples had no significant deformations after 30 cyclic compressions except (PGS-co-60PEG2)-M, which broke after 13 cyclic compressions in dry and 10 cyclic compressions in swollen conditions (Figs. S15 and S16 Supporting Information). Other samples, the same as (PGS-co-40PEG2)-M, as shown in the inserted illustrations of Fig. 5D–F, displayed nearly overlapped loading-unloading curves and no significant stress shift during the compression period in the 30-cycle compressive test with 40% applied strain. The scaffolds were subjected to a compression of 40% of their original height and then returned to their initial state upon release of the pressure (Video 3 and 4 Supporting Information). The reversibility after one load-unload and 30 cyclic load-unload cycles for all samples was almost 100%, except for (PGS-co-60PEG2)-M.

The obtained values of Young's modulus of (PGS-co-PEG2)-M samples were in the range of soft tissues like skin, adipose, myocardial, cartilage and nerve, which is advantageous for soft tissue engineering [16,46,53–55], while (PGS-co-20PEG3)-M and (PGS-co40PEG3)-M specimens were in the range of hard tissues [27,37,56] (Video 1 to 4 Supporting Information). As a result, (PGS-co-PEG)-M copolymers could be used for both soft tissues and hard tissues, which expands the potential biomedical applications of PGS.

3.9. Lap-shear strength

In the lap shear test, adhesion is evaluated under shear deformations [28]. Shear stresses were measured over several ranges, with appropriate controllability and repeatability (Fig. 6B). Among the (PGS-co--PEG)-M samples, (PGS-co-60PEG2)-M had the highest shear strength (122.01 ± 29.12 kPa), and the second highest shear strength was 94.80 ± 12.05 kPa for (PGS-co-60PEG3)-M. Increasing PEG concentrations led to significant increases in shear strengths (*$P < 0.05$ and **$P < 0.01$) (Fig. 6B), and the strengths of lap-shear for (PGS-co-PEG2)-M was greater than that of (PGS-co-PEG3)-M. As can be seen, the lowest shear strengths were for pure PGS-M and (PGS-co-20PEG3)-M, but compared to our previous study on non-methacrylate PGS-co-PEG copolymers [22], all the methacrylate copolymers showed lap-shear strengths higher than 10 kPa; however, after methacrylation, the shear strengths were remarkably reduced ($P < 0.01$). The lap-shear strengths of (PGS-co--PEG)-M were in the range that could be considered as adhesive, and (PGS-co-60PEG2)-M and (PGS-co-60PEG3)-M had higher values than CoSeal (~69 kPa), a commercially available biosealants [57,58]. Adhesive polymers typically contain hydrophilic groups, such as hydroxyls, carboxyls, amides, and sulphates, which are known as adhesively active groups. These groups enable them to attach to different surfaces via hydrogen bonding, hydrophilic interaction, or electrostatic attraction. PEG is FDA-approved and is already widely used in biomedicine due to its cytocompatibility. Adhesives made from PEG have been established and commercialised for use as tissue sealants (e.g., CoSeal™ and DuraSeal™) [28,59–61]. Also, PEGylation is a common technique for developing bioadhesives to conjugate PEG chains with specific molecules [28,62]. These results demonstrate that adding PEG to PGS resulted in an increase in adhesive properties and hydrophilicity, and even after methacrylation, and (PGS-co-PEG)-M copolymers contained these characteristics. It is worth mentioning that methacrylate samples, (PGS-co-PEG3)-M particularly, were less adhesive and hydrophilic than their non-methacrylated counterparts. This observed decrease may be attributed to the presence of methacrylic groups, which substitute hydroxyl groups. As discussed earlier, (PGS-co-PEG3)-M had a higher degree of methacrylation than (PGS-co-PEG2)-M, and (PGS-co-PEG2)-M showed greater adhesive behaviours than others; therefore, this difference can be correlated to methacrylic group substitutions.

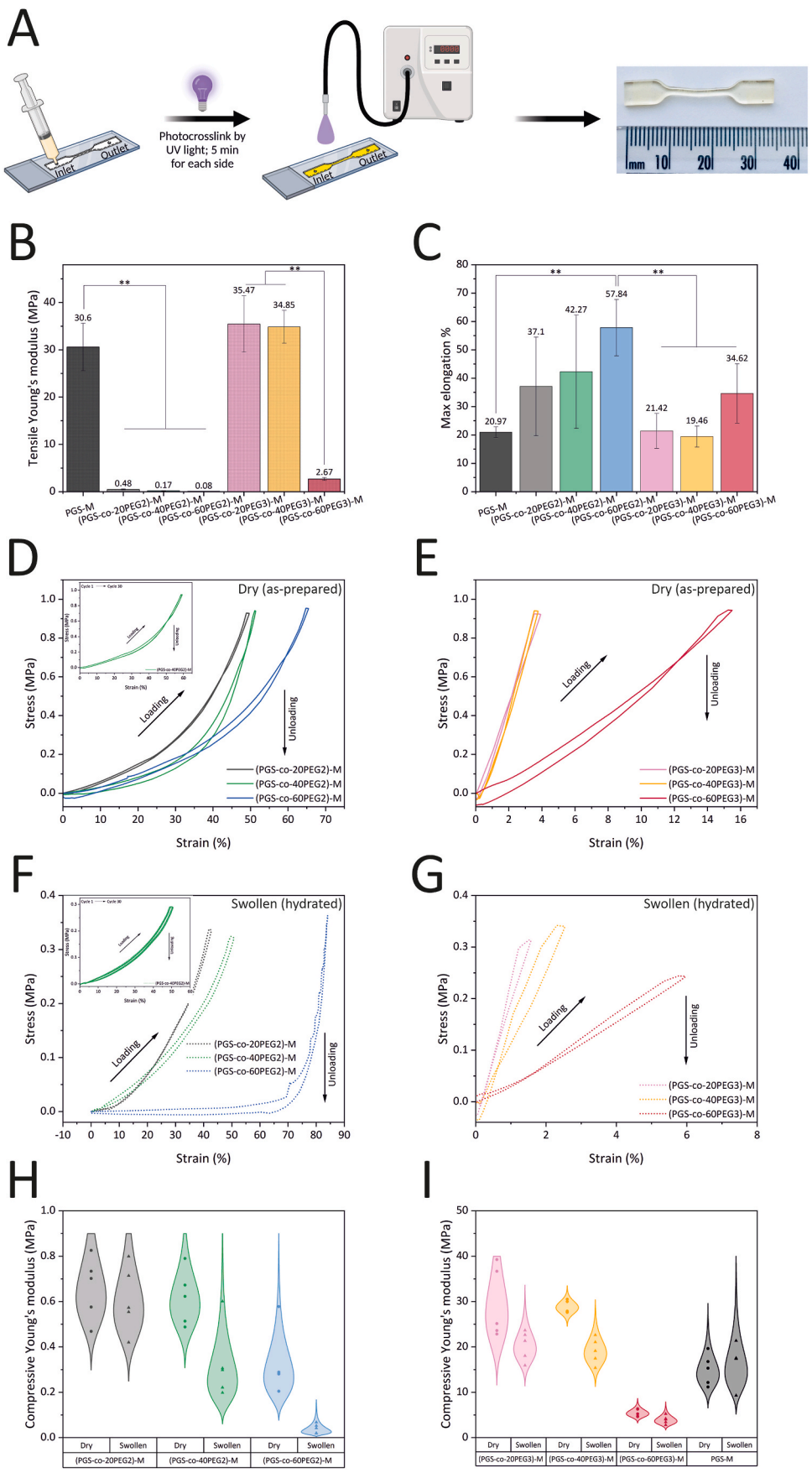

Fig. 5. Mechanical properties of (PGS-co-PEG2)-M and (PGS-co-PEG3)-M were analysed by tensile (A, B and C) and compression test (D to I). Tensile test: (A) A schematic of preparing (PGS-co-PEG)-M copolymers in dog-bone shape by injecting photocurable copolymer solution containing PI to a dog-bone shape PDMS mould and photocrosslinking under UV light for 10 min. (B) Tensile Young's modulus and (C) max elongation percentages of (PGS-co-PEG2)-M and (PGS-co-PEG3)-M copolymers. Data are means ± SD (n = 5; **P < 0.01). Compression test: One-cycle load-unload compressive stress-strain curves of the dry (PGS-co-PEG2)-M (D) and (PGS-co-PEG3)-M (E) and swollen (PGS-co-PEG2)-M (F) and (PGS-co-PEG3)-M (G). The inserted illustrations (top left corner of D and F) depict the cyclic stress-strain curves of dry and swollen (PGS-co-40PEG2)-M after undergoing 30 cyclic compressions. Compressive Young's modulus of (PGS-co-PEG2)-M (H) and (PGS-co-PEG3)-M (I) in dry and swollen conditions.

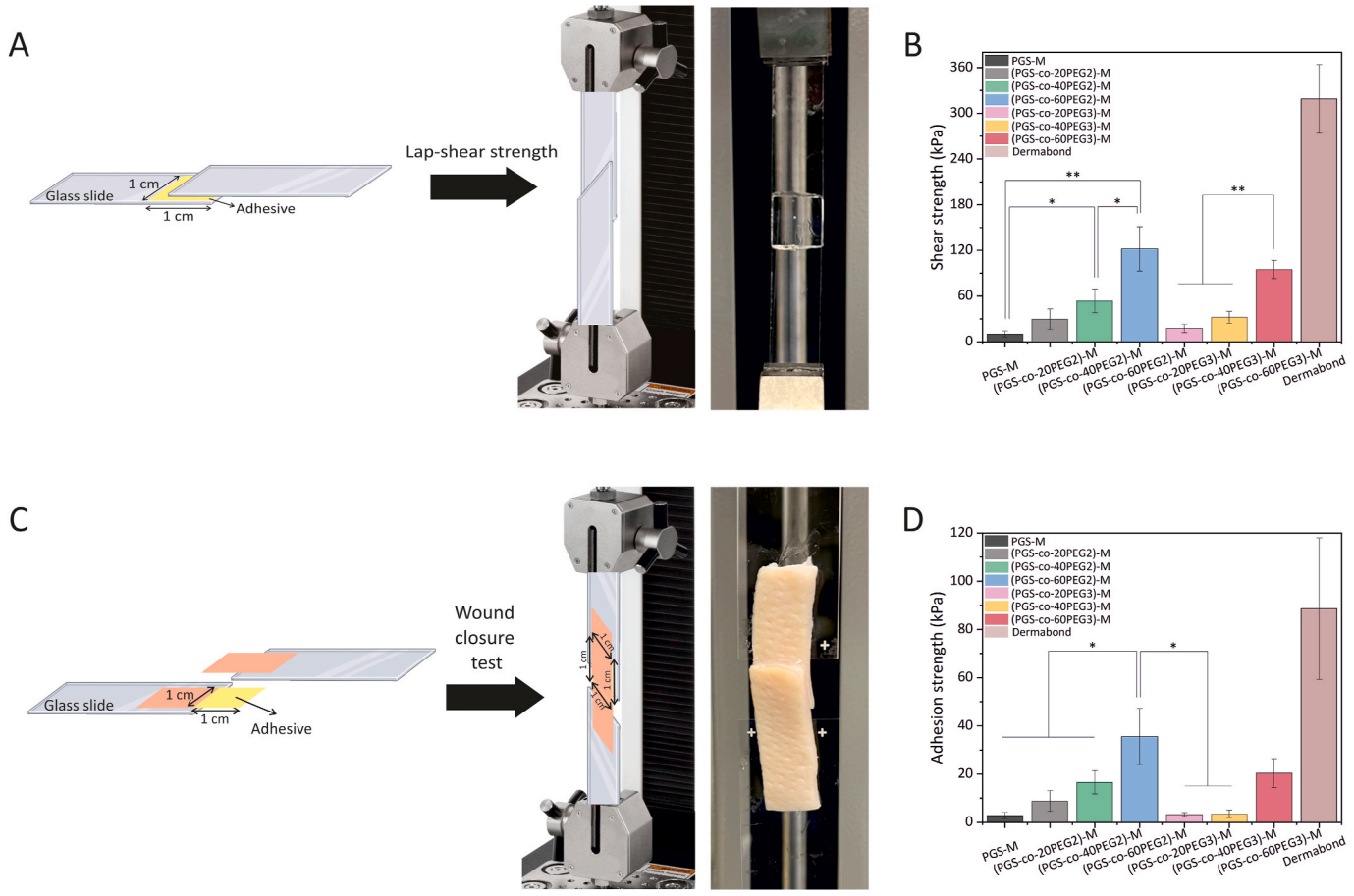

Fig. 6. (A) The modified assay for measuring lap-shear strength (ASTMF2255-05) is shown schematically and (B) the average shear strengths of (PGS-co-PEG)-M adhesives made of two different types of PEG and three different concentrations. Dermabond™ was used as a control. Data are means ± SD (n = 5; *P < 0.05 and **P < 0.01). The adhesion properties of (PGS-co-PEG)-M copolymers have been evaluated in vitro using freshly harvested porcine skin: (C) Schematic and picture of the modified test for wound closure test (ASTM F2458-05) and (D) results of adhesive strengths of (PGS-co-PEG)-M including different PEG types and concentrations. Data are means ± SD (n = 5; *P < 0.05).

3.10. Wound closure test

According to ASTM standard F2458-05, wound closure tests (a technique used to reproduce pulling/stretching forces) were conducted on (PGS-co-PEG)-M samples using freshly harvested porcine skin to evaluate their adhesion (Fig. 6C). With increasing PEG concentration, adhesive strength increased, and the increase was greater in (PGS-co-PEG2)-M copolymers compared to (PGS-co-PEG3)-M copolymers. PGS-M, (PGS-co-20PEG3)-M, and (PGS-co-40PEG3)-M had no significant statistical differences in their adhesion properties (~3 kPa). In contrast, the highest value of adhesion strength was 35.60 ± 11.63 kPa for (PGS-co-60PEG2)-M among (PGS-co-PEG2)-M samples (Video 5 Supporting Information), while among (PGS-co-PEG3)-M specimens 20.40 ± 5.94 kPa was highest for (PGS-co-60PEG3)-M. Compared to the reported adhesive strength of Progel (~10 kPa), CoSeal (~19 kPa), Evicel (~26 kPa), Quixil (24.6 kPa), Beriplast (24.2 kPa) and Kryptonite (~30 kPa), (PGS-co-40PEG2)-M, (PGS-co-60PEG2)-M and (PGS-co-60PEG3)-M had similar adhesion strength [57,63–65]. However, Tachosil (59.6 kPa), Tisseel (77.5 kPa) [63] and Dermabond™ (~88.6 kPa, tested in this study as a control) reached higher adhesive strength than (PGS-co--PEG)-M samples. Compared to our previous study, the adhesive strengths of (PGS-co-PEG)-M samples, methacrylate samples, were noticeably lower (P < 0.05) than non-methacrylate PGS-co-PEG co-polymers [22]. Adhesive properties are crucial for bioglue, wound dressings, and implanted biomaterials because they promote biointegration and prevent detachment [64,66]; therefore, they may be promising for the mentioned applications, particularly for soft tissues.

3.11. Adhesion test with different substrates and stainless steel calibration weights

To further explore the adhesive properties seen in relation to the addition of PEG concentration, and particularly those samples containing PEG2 more tests were performed. The most adhesive sample, (PGS-co-60PEG2)-M, demonstrated an adhesive behaviour on different inorganic materials, including polystyrene, silicone, glass, polypropylene polyethylene terephthalate, stainless steel, wood, polytetrafluoroethylene and aluminium using those objects that are commonly used in the laboratory (Fig. 7). The density of surface hydrogen-bonding groups determines the properties of polymer adhesives, according to Faghihnejad et al. [67]. Therefore, (PGS-co-60PEG2)-M had a higher density of surface hydrogen-bonding groups among other samples and could provide a range of adhesive properties. Also, Van der Waals forces and dipole-dipole interactions can lead to enhanced adhesion [28]. In addition, mechanical interlock(s) between adhesive polymer and the surface irregularities or microstructures of the substrates is another reason for adhesion [28]. Adhesive polymers that exhibit good flexibility have the ability to conform to the irregularities or microscale roughness found on substrate surfaces. The ability of the adhesive to conform to the substrate surfaces results in an increased contact area and

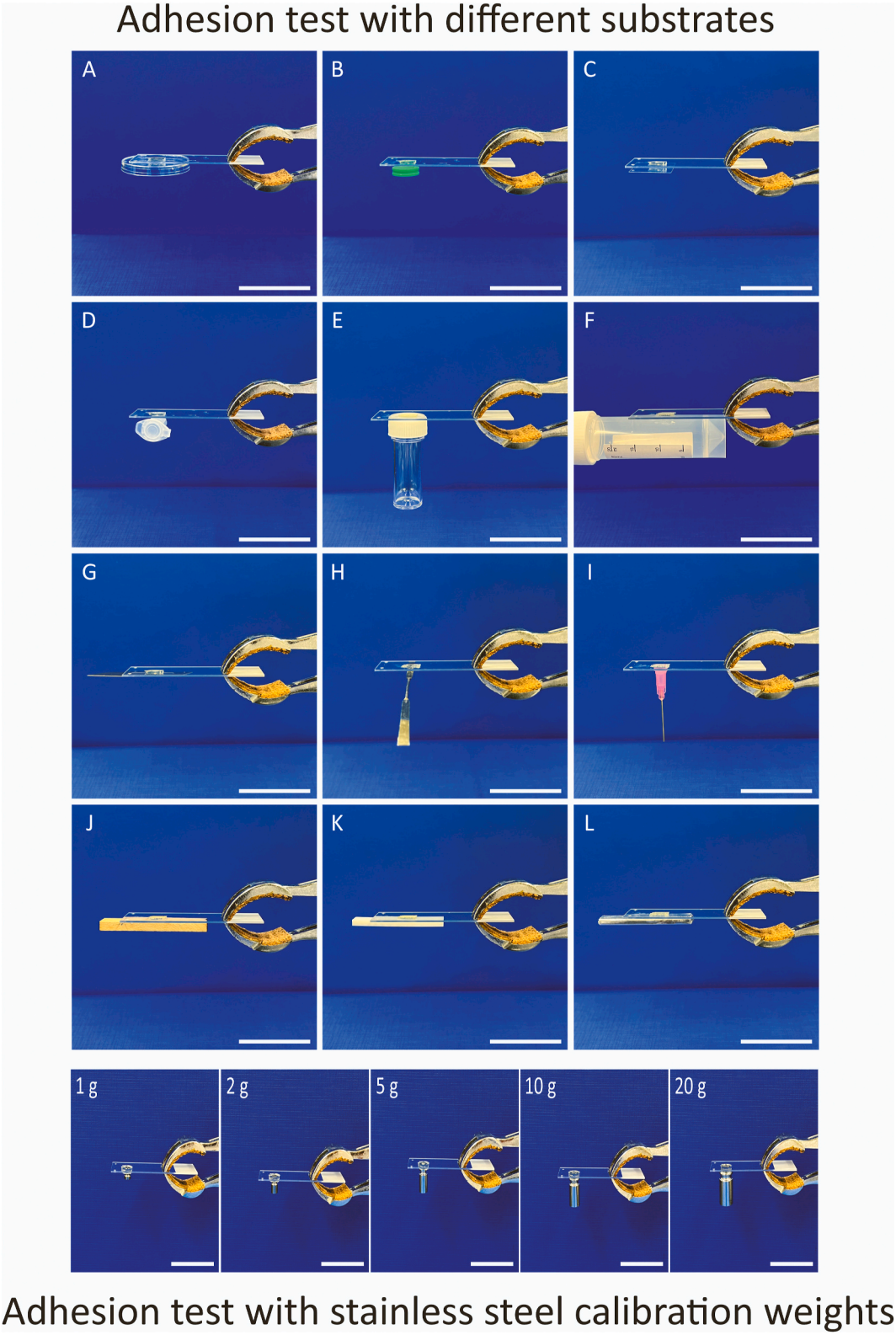

Fig. 7. Adhesive performance of (PGS-co-60PEG2)-M sample (5 mm × 10 mm) with different substrates: Pictures of adhesion to (A) petri dish (polystyrene), (B) rubber plunger (silicone), (C) coverslips (glass), (D) Eppendorf tubes (polypropylene), (E) Bijou (polystyrene), (F) 20 ml centrifuge tube (polyethylene terephthalate), (G) scalpel blade (hardened-tempered stainless steel), (H) spatula (stainless steel), (I) needle 18G (plastic end, polypropylene), (J) wood, (K) polytetrafluoroethylene and (L) aluminium. Scale bar = 37 mm. Pictures of 1 g, 2 g, 5 g, 10 g and 20 g stainless steel calibration weights adhered to a 12 mm diameter of (PGS-co-60PEG2)-M. Scale bar = 37 mm.

enhanced interfacial adhesion, ultimately improving the bonding strength [28,65]. (PGS-co-60PEG2)-M can manifest high cohesion and strong interfacial adhesion, which contributes to stable adhesion to various substrates [68]. Based on the results, it can be said that (PGS-co-60PEG2)-M has relatively strong adhesion, and due to having ~35 kPa adhesion strength, it can adhere to most metals and coatings (adhesion strength between 25 and 40 kPa is needed) [69].

Also, several stainless steel calibration weights were used to evaluate how long the sample, a circular shape with a 12 mm diameter of (PGS-co-60PEG2)-M, could support the weights without falling off (Fig. 7). The (PGS-co-60PEG2)-M could support 1 g, 2 g, 5 g, 10 g, and 20 g of stainless steel calibration weight for more than 1 h without falling off, 50 g and 100 g weights were held for 15–30 s (PGS-co-60PEG2)-M is flexible and soft, and due to its transparency, lightweight, and adhesive properties, it has potential uses as an adhesive sensor or flexible device in medical applications [70,71].

3.12. Cell attachment, proliferation and viability

3.12.1. Cell attachment

To evaluate the cell attachment of HaCaT cells on (PGS-co-PEG)-M copolymers and PGS-M, the cell metabolic activity was assessed by resazurin assay on day 1. On the first day, when cells have undergone at most one round of cell doubling, assessing cell metabolic activity can provide information about cell attachment. As can be seen in Fig. 8A, higher concentrations of PEG, either PEG2 or PEG3, resulted in greater cell metabolic activities [22,24]; however, the percentages of cell metabolic activity were higher for (PGS-co-PEG2)-M compared to (PGS-co-PEG3)-M samples. This result could be related to the hydrophilicity and degree of crosslinking density in specimens since, in previous sections, it was shown that (PGS-co-PEG2)-M copolymers were more hydrophilic and had lower degrees of crosslinking.

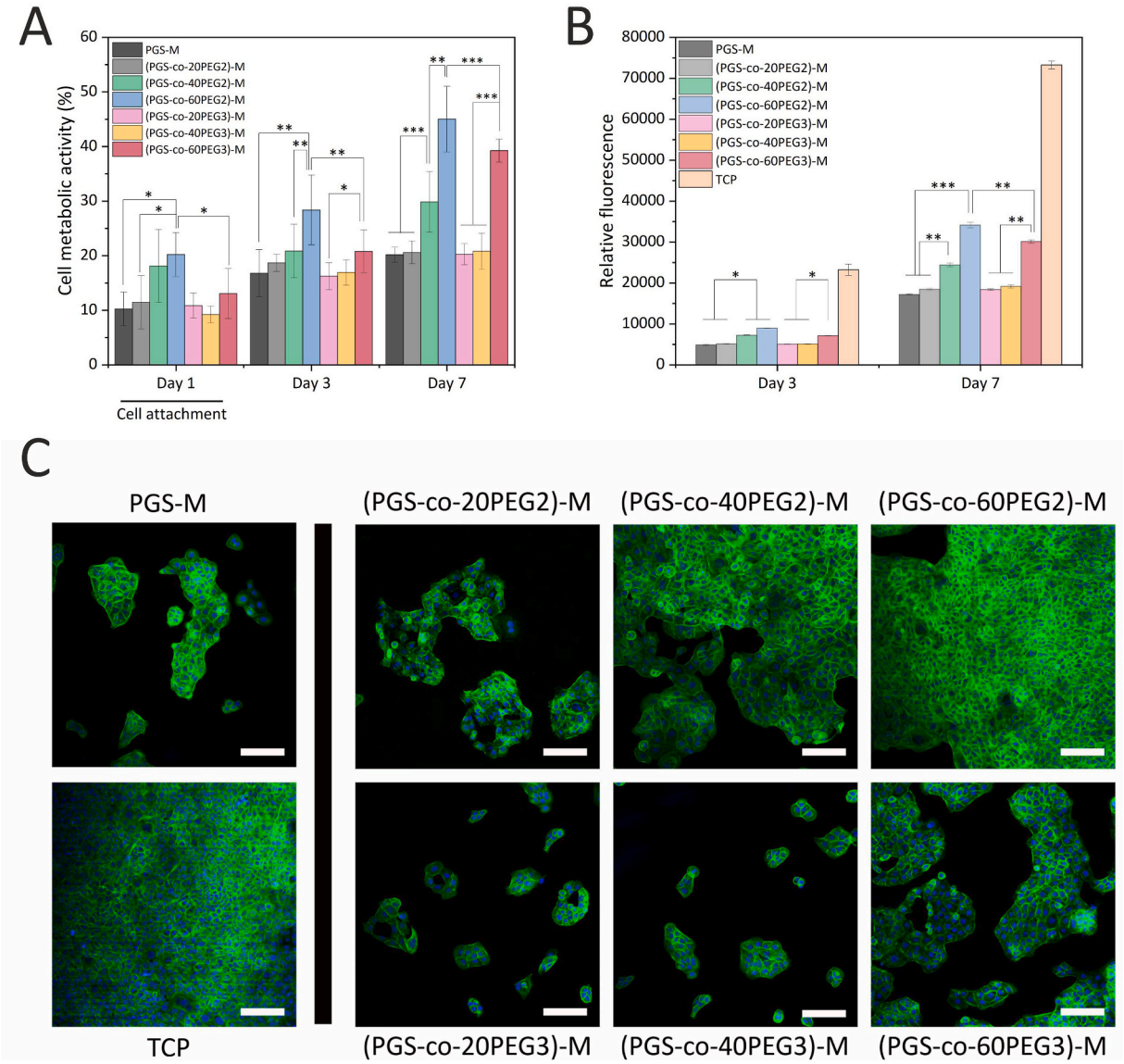

Fig. 8. (A) Results of resazurin assays from seeded HaCaT cells on (PGS-co-PEG)-M and PGS-M samples on day 1, 3 and 7. The results are reported in percentage and normalised by positive control, tissue culture plate (TCP) (n = 5; *P < 0.05, **P < 0.01 and ***P < 0.001). (B) PicoGreen® assay for dsDNA content of HaCaT cells on (PGS-co-PEG)-M surfaces on day 3 and day 7. Positive controls were HaCaT cells cultured on TCP. Also, PGS-M was a control (n = 5; *P < 0.05, **P < 0.01 and ***P < 0.001). The formula used for calculating the number of cells was obtained from the calibration curve using a polynomial trendline: $y = 2\text{ E-}06 \times^{2} + 0.1621x + 2320.3$ with $R^2 = 0.9957$. (C) Fluorescent staining of HaCaT cells cultured on PGS-M and (PGS-co-PEG)-M samples after being cultured for 3 days (Scale bar represents 150 μm, blue: DAPI, green: Phalloidin FITC).

3.12.2. Cell proliferation and viability

Cell metabolic activity was measured at day 3 and day 7 in order to investigate adherent HaCaT cell proliferation and viability on (PGS-co-PEG)-M and PGS-M (Fig. 8A). Once cells can undergo multiple cell doublings (over an extended period like on day 3 and day 7), this assay provides more information on the impact of the material on cell proliferation. On day 3, the samples with higher concentrations of PEG had higher cell metabolic activities [22], with (PGS-co-60PEG2)-M having the highest percentage, reaching 28.39 ± 6.40%, followed by, (PGS-co-60PEG3)-M with 20.80 ± 3.92%. From day 3 to day 7, the cell metabolic activities of both (PGS-co-PEG2)-M and (PGS-co-PEG3)-M increased in a significant statistically manner (a two-way analysis of variance (ANOVA); $P < 0.05$), and the highest values were 45.05 ± 6.00% and 39.26 ± 2.10% for (PGS-co-60PEG2)-M and (PGS-co-60-PEG3)-M, respectively (day 7). Therefore, it can be said that HaCaT cells had higher proliferation and viability on (PGS-co-60PEG2)-M and (PGS-co-60PEG3)-M than others on day 3 and day 7. As a result of adding PEG, the hydrophilicity of the copolymers increases, resulting in improved surface for cell growth [11,22,24,52]. In vivo and in vitro, PGS has been studied for various tissue engineering applications because of its cytocompatibility [5,72,73]; as a result of resazurin assay, (PGS-co-PEG)-M, samples containing PEG ≥40% in particular, may also be suitable candidates for use in biomedicine since they showed a good range of cytocompatibility.

3.13. PicoGreen® assay

PicoGreen® DNA quantification assay was used to quantify the number of HaCaT cells present on the (PGS-co-PEG)-M surfaces in the culture at day 3 and day 7. In this assay, the amount of dsDNA present in each sample was measured by relative fluorescence (RF). A standard curve was then used to calculate the number of cells present [15,74]. Among (PGS-co-PEG)-M samples, those containing 40% and 60% of PEG, either PEG2 or PEG3, had higher RFs; for instance, the RF of (PGS-co-60PEG2)-M > (PGS-co-40PEG2)-M ≃ (PGS-co-60PEG3)-M on day 3 (Fig. 8B). (PGS-co-60PEG2)-M on both days showed the highest fluorescent values among other (PGS-co-PEG)-M samples; its RF was 8979.28 ± 51.53 (equals ~30,323 HaCaT cells) and was 34152.32 ± 647.01 (equals ~87,503 HaCaT cells) on day 3 and day 7, respectively. On day 3, the RF of (PGS-co-60PEG3)-M (7180.96 ± 56.30; equals ~26,239 HaCaT cells) was very similar to (PGS-co-40PEG2)-M (7273.52 ± 73.35; equals ~26,449 HaCaT cells); however, on day 7, the RF of (PGS-co-60PEG3)-M enhanced significantly (30145.4 ± 405.25; equals ~78,402 HaCaT cells) ($P < 0.01$), remarkably higher than (PGS-co-40-PEG2)-M (24422.52 ± 475.68; equals ~65,402 HaCaT cells). Also, PGS-M, (PGS-co-20PEG2)-M, (PGS-co-20PEG3)-M and (PGS-co-40PEG3) had similar RF values on day 3, 4897.6 ± 154.25 (equals ~21,052 HaCaT cells), 5181.08 ± 26.40 (equals ~21,696 HaCaT cells), 5086.4 ± 26.19 (equals ~21,481 HaCaT cells) and 5119.52 ± 56.03 (equals ~21,556 HaCaT cells), respectively. After four days, on day 7, all these four samples had a significant increase in RF amounts, which can be related to increasing the number of HaCaT cells over time. As can be seen in Fig. 8B, the obtained RF was increased noticeably for all samples from day 3 to day 7 (a two-way analysis of variance (ANOVA); $P < 0.01$). A similar trend was observed in resazurin results, which measures the metabolic activity of the total cell population. Given the strong observed correlation between PicoGreen and resazurin results, it is likely that the increase in both assays for higher percentages of PEG in (PGS-co-PEG)-M samples indicates an increase in cell proliferation and growth over time. It is worth mentioning that according to the results, all photocrosslinked specimens, PGS-M and (PGS-co-PEG)-M, have been shown to support the growth of HaCaT cells, although this was lower than on TCP (positive control).

3.14. Immunofluorescence staining

HaCaT cells were observed growing on PGS-M and (PGS-co-PEG)-M samples using an LSM880 AiryScan Confocal Microscope (ZEISS, Germany), with cells stained with DAPI and FITC-Phalloidin after 3 days. For all fluorescent images, DAPI was used to stain the nuclei, and FITC-Phalloidin was used to stain the F-actin (Fig. 8C). On PGS-M, (PGS-co-PEG2)-M, and (PGS-co-PEG3)-M HaCaT cells were seen to have a cubical shape on day 3 [75]. It was easier to determine the morphology of HaCaT cells on samples with less cells, such as PGS-M, (PGS-co-20-PEG2)-M, and (PGS-co-20PEG3)-M (Fig. 8C). Copolymers with higher PEG concentrations showed better cell adhesion, such as (PGS-co-40-PEG2)-M, (PGS-co-60PEG2)-M and (PGS-co-60PEG3)-M. The enhanced adhesion of HaCaT cells to (PGS-co-PEG)-M elastomers can be explained by the increase in surface wettability when PEG, either PEG2 or PEG3, was copolymerised, particularly for higher percentages of PEG (PEG ≥40%). Likewise, the resazurin and PicoGreen results showed the same trend: a higher PEG concentration led to more metabolic activity and higher growth in HaCaT cells [22]. Consequently (PGS-co-PEG),-M copolymers could support cell attachment and proliferation, making them suitable for different biomedical applications.

3.15. Applications and future plans

By making PGS-co-PEG copolymers photocurable and developing (PGS-*co*-PEG)-M in this study, we are improving the processability of these materials and so facilitating and broadening their use for biofabrication [76,77]. The capability of (PGS-co-PEG)-M to crosslink rapidly within a couple of minutes, aiding in the creation of more complex scaffolds than can be achieved using conventional thermal curing, brought methacrylation to the forefront. These photocurable copolymers can be used in various biofabrication techniques, such as emulsion-based templating (Fig. S17 Supporting Information) and additive manufacturing (either direct or indirect) (Fig. 9). (PGS-co-PEG)-M copolymers no longer require harsh conditions to crosslink, so they become suitable for adding biomolecules and cells before crosslinking that the harsh conditions would destroy. Also, because these polymers are soluble in water to some extent [22,43], there would be a possibility of developing bioinks based on them. Furthermore, due to different ranges of properties, (PGS-co-PEG)-M can be used to replace and repair various organs and tissues; also, by changing the degree of methacrylation and making composites out of them, the characteristics can be tuned based on a target application. For example, (PGS-co-60PEG2)-M is flexible, soft, transparent, adhesive and light, making it suitable for biomedical applications such as an adhesive sensor, flexible device or wound dressing.

4. Conclusion

(PGS-co-PEG2)-M and (PGS-co-PEG3)-M were successfully synthesised and methacrylated to develop photocurable PGS-co-PEG copolymers, and after methacrylation, they were evaluated physically, chemically and biologically by conducting a comprehensive range of assays. Chemical analysis (FTIR and NMR) confirmed the addition of methacrylate groups by analysing the peaks associated with them. As a result of methacrylation, mechanical properties were significantly altered, particularly for (PGS-co-PEG3)-M; however, the lap-shear and adhesion strengths of (PGS-co-PEG)-M noticeably decreased compared to PGS-co-PEG. According to the results, photocrosslinking of (PGS-co-PEG)-M copolymers induced higher crosslinking density than thermally cured PGS-co-PEG (previously published study). Furthermore, due to the PEG3 structure, there are more methacrylic groups in (PGS-co-PEG3)-M

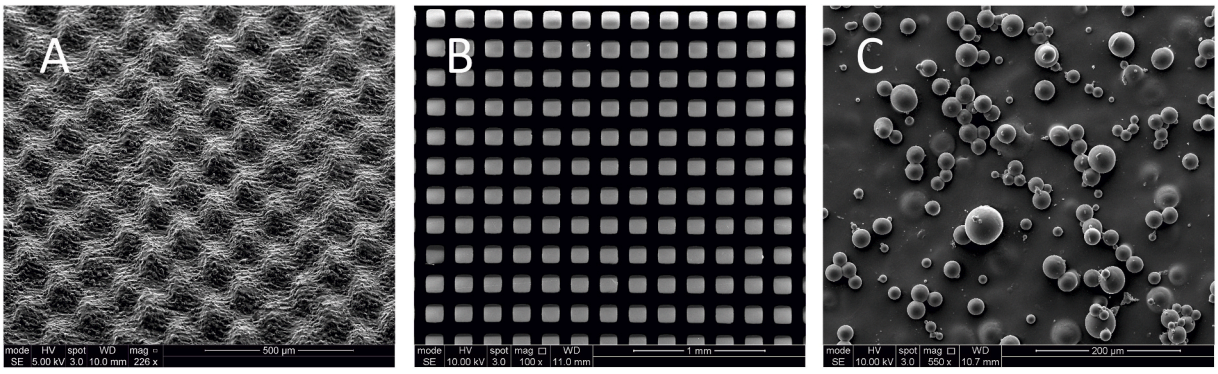

Fig. 9. SEM images of (PGS-co-60PEG3)-M with different structures using two biofabrication techniques: (A) and (B) indirect 3D printing using Form 2, FormLabs and MicroSLA-15 and (C) emulsion polymerisation to produce non-porous microspheres (Fig. S17 Supporting Information).

than in (PGS-co-PEG2)-M; therefore, (PGS-co-PEG3)-M had higher crosslinking density than (PGS-co-PEG2)-M. Similar to PGS-co-PEG, after the functionalisation, the (PGS-co-PEG)-M samples showed a good range of cytocompatibility, and there was a direct relationship between PEG concentration and cytocompatibility; specimens including higher percentages of PEG had higher cytocompatibility.

Author contributions

Mina Aleemardani: conceptualisation, investigation, methodology, validation, funding acquisition, writing – original draft. Louis Johnson: investigation, drawing figures, writing – review & editing. Michael Zivojin Trikić;: investigation, methodology, supervision, writing – review & editing. Nicola Helen Green: conceptualisation, investigation, methodology, validation, funding acquisition, supervision, writing – review & editing. Frederik Claeyssens: conceptualisation, investigation, methodology, validation, funding acquisition, supervision, writing – review & editing.

Declaration of competing interest

The authors declare that they have no known competing financial interests or personal relationships that could have appeared to influence the work reported in this paper.

Data availability

Data will be made available on request.

Acknowledgements

The authors acknowledge the financial assistance provided to Mina Aleemardani by the University of Sheffield. The authors would like to thank the EPSRC funded Centre for Doctoral Training in Advanced Biomedical Materials grant reference EP/S022201/1 provided to Louis Johnson. Frederik Claeyssens also thanks the Royal Society for funding of a Royal Society Leverhulme Trust Senior Research Fellowship 2022 (SRF\R1\221053). Many thanks to the EPSRC (grant EP/I007695/1) and the Medical Research Council (grant MR/L012669/1) for their support and funding of the equipment used in this study. Confocal imaging work was performed at the Wolfson Light Microscopy Facility, using the ZEISS LSM880 AiryScan confocal microscope. Special thanks to ARMOURERS & BRASIERS' COMPANY and UK Tissue and Cell Engineering Society (TCES) for their support in presenting this work. Thanks to Boyang Liu, Rachel Furmidge, Dr Lisa Hollands and Dr Nicholas J Van Hateren for their help during this study.

Appendix A. Supplementary data

Supplementary data to this article can be found online at https://doi.org/10.1016/j.mtadv.2023.100410.

References

[1] M.H. Aghajan, M. Panahi-Sarmad, N. Alikarami, S. Shojaei, A. Saeidi, H. A. Khonakdar, M. Shahrousvan, V. Goodarzi, Using solvent-free approach for preparing innovative biopolymer nanocomposites based on PGS/gelatin, Eur. Polym. J. 131 (2020), 109720.
[2] M. Heydari, V. Goodarzi, M. Shams, N.M. Kazemi, A. Salimi, The role of copper chromite nanoparticles on physical and bio properties of scaffolds based on poly (glycerol-azelaic acid) for application in tissue engineering fields, Cell Tissue Res. 391 (2023) 357–373.
[3] X.J. Loh, A.A. Karim, C. Owh, Poly (glycerol sebacate) biomaterial: synthesis and biomedical applications, J. Mater. Chem. B 3 (2015) 7641–7652.
[4] L. Vogt, F. Ruther, S. Salehi, A.R. Boccaccini, Poly (glycerol sebacate) in biomedical applications—a review of the recent literature, Adv. Healthc. Mater. 10 (2021), 2002026.
[5] Z. Wu, K. Jin, L. Wang, Y. Fan, A review: optimization for poly (glycerol sebacate) and fabrication techniques for its centered scaffolds, Macromol. Biosci. 21 (2021), 2100022.
[6] J.M. Kemppainen, S.J. Hollister, Tailoring the mechanical properties of 3D-designed poly (glycerol sebacate) scaffolds for cartilage applications, J. Biomed. Mater. Res. Part A An Off. J. Soc. Biomater. Japanese Soc. Biomater. Aust. Soc. Biomater. Korean Soc. Biomater. 94 (2010) 9–18.
[7] C.L.E. Nijst, J.P. Bruggeman, J.M. Karp, L. Ferreira, A. Zumbuehl, C.J. Bettinger, R. Langer, Synthesis and characterization of photocurable elastomers from poly (glycerol-co-sebacate), Biomacromolecules 8 (2007) 3067–3073.
[8] I.C. Becerril-Rodriguez, F. Claeyssens, Low methacrylated poly (glycerol sebacate) for soft tissue engineering, Polym. Chem. 13 (2022) 3513–3528.
[9] R. Qu, D. Zhou, T. Guo, W. He, C. Cui, Y. Zhou, Y. Zhang, Z. Tang, X. Zhang, Q. Wang, 4D printing of shape memory inferior vena cava filters based on copolymer of poly (glycerol sebacate) acrylate-co-hydroxyethyl methacrylate (PGSA-HEMA), Mater. Des. 225 (2023), 111556.
[10] S. Seyfikar, M. Asgharnejad-laskoukalayeh, S.H. Jafari, V. Goodarzi, M.H. Salehi, S. Zamanlui, Introducing a new approach to preparing bionanocomposite sponges based on poly (glycerol sebacate urethane)(PGSU) with great interconnectivity and high hydrophilicity properties for application in tissue engineering, Eur. Polym. J. 173 (2022), 111239.
[11] Z. Wang, Y. Ma, Y. Wang, Y. Liu, K. Chen, Z. Wu, S. Yu, Y. Yuan, C. Liu, Urethane-based low-temperature curing, highly-customized and multifunctional poly (glycerol sebacate)-co-poly (ethylene glycol) copolymers, Acta Biomater. 71 (2018) 279–292.
[12] Y. Ma, C. Zhang, Y. Wang, L. Zhang, J. Zhang, J. Shi, J. Si, Y. Yuan, C. Liu, Direct three-dimensional printing of a highly customized freestanding hyperelastic bioscaffold for complex craniomaxillofacial reconstruction, Chem. Eng. J. 411 (2021), 128541.
[13] P. Ghaffari-Bohlouli, H. Golbaten-Mofrad, N. Najmoddin, V. Goodarzi, A. Shavandi, W.-H. Chen, Reinforced conductive polyester based on itaconic acids, glycerol and polypyrrole with potential for electroconductive tissue restoration, Synth. Met. 293 (2023), 117238.
[14] Y.-L. Wu, A.R. D'Amato, A.M. Yan, R.Q. Wang, X. Ding, Y. Wang, Three-dimensional printing of poly (glycerol sebacate) acrylate scaffolds via digital light processing, ACS Appl. Bio Mater. 3 (2020) 7575–7588.
[15] S. Pashneh-Tala, R. Owen, H. Bahmaee, S. Rekštytė, M. Malinauskas, F. Claeyssens, Synthesis, characterization and 3D micro-structuring via 2-photon polymerization of poly (glycerol sebacate)-methacrylate–an elastomeric degradable polymer, Front. Physiol. 6 (2018) 41.

[16] D. Singh, A.J. Harding, E. Albadawi, F.M. Boissonade, J.W. Haycock, F. Claeyssens, Additive manufactured biodegradable poly (glycerol sebacate methacrylate) nerve guidance conduits, Acta Biomater. 78 (2018) 48–63.
[17] M.F.V. de la Paz, M. Aleemardani, R. Furmidge, S. Pashneh-Tala, F. Claeyssens, Effect of solvent type on porous structure of emulsion templated poly (glycerol sebacate)-methacrylate, Mater. Lett. (2023), 134566.
[18] Y.-C. Yeh, C.B. Highley, L. Ouyang, J.A. Burdick, 3D printing of photocurable poly (glycerol sebacate) elastomers, Biofabrication 8 (2016), 45004.
[19] S. Pashneh-Tala, R. Moorehead, F. Claeyssens, Hybrid manufacturing strategies for tissue engineering scaffolds using methacrylate functionalised poly (glycerol sebacate), J. Biomater. Appl. 34 (2020) 1114–1130.
[20] J. Field, J.W. Haycock, F.M. Boissonade, F. Claeyssens, A tuneable, photocurable, poly (caprolactone)-based resin for tissue engineering—synthesis, characterisation and use in stereolithography, Molecules 26 (2021) 1199.
[21] L. Yu, G. Zeng, J. Xu, M. Han, Z. Wang, T. Li, M. Long, L. Wang, W. Huang, Y. Wu, Development of poly (glycerol sebacate) and its derivatives: a review of the progress over the past two decades, Polym. Rev. (2022) 1–66.
[22] M. Aleemardani, M.Z. Trikic, N.H. Green, F. Claeyssens, Elastomeric, bioadhesive and pH-responsive amphiphilic copolymers based on direct crosslinking of poly (glycerol sebacate)-co-polyethylene glycol, Biomater. Sci. 10 (2022) 7015–7031.
[23] D. Lin, B. Cai, L. Wang, L. Cai, Z. Wang, J. Xie, Q. Lv, Y. Yuan, C. Liu, S.G.F. Shen, A viscoelastic PEGylated poly (glycerol sebacate)-based bilayer scaffold for cartilage regeneration in full-thickness osteochondral defect, Biomaterials 253 (2020), 120095.
[24] Y.-T. Tsai, C.-W. Chang, Y.-C. Yeh, Formation of highly elastomeric and property-tailorable poly (glycerol sebacate)-co-poly (ethylene glycol) hydrogels through thiol–norbornene photochemistry, Biomater. Sci. 8 (2020) 4728–4738.
[25] T.-L. Cheng, K.-H. Chuang, B.-M. Chen, S.R. Roffler, Analytical measurement of PEGylated molecules, Bioconjugate Chem. 23 (2012) 881–899.
[26] A. Nag, G. Mitra, P.C. Ghosh, A colorimetric assay for estimation of polyethylene glycol and polyethylene glycolated protein using ammonium ferrothiocyanate, Anal. Biochem. 237 (1996) 224–231.
[27] M. Aleemardani, A. Solouk, S. Akbari, M. Moeini, A hydrogel–fiber–hydrogel composite scaffold based on silk fibroin with the dual-delivery of oxygen and quercetin, Biotechnol. Bioeng. 120 (2023) 297–311.
[28] H. Montazerian, E. Davoodi, A. Baidya, M. Badv, R. Haghniaz, A. Dalili, A. S. Milani, M. Hoorfar, N. Annabi, A. Khademhosseini, Bio-macromolecular design roadmap towards tough bioadhesives, Chem. Soc. Rev. 51 (2022) 9127–9173.
[29] A.H.C. Anthis, X. Hu, M.T. Matter, A.L. Neuer, K. Wei, A.A. Schlegel, F.H. L. Starsich, I.K. Herrmann, Chemically stable, strongly adhesive sealant patch for intestinal anastomotic leakage prevention, Adv. Funct. Mater. 31 (2021), 2007099.
[30] D. Rana, T. Colombani, B. Saleh, H. Mohammad, N. Annabi, S.A. Bencherif, Engineering injectable, biocompatible, and highly elastic bioadhesive cryogels, Mater. Today Bio (2023), 100572.
[31] H. Montazerian, A.H. Najafabadi, E. Davoodi, R. Seyedmahmoud, R. Haghniaz, A. Baidya, W. Gao, N. Annabi, A. Khademhosseini, P.S. Weiss, Poly-catecholic functionalization of biomolecules for rapid gelation, robust injectable bioadhesion, and near-infrared responsiveness, Adv. Healthc. Mater. (2023), 2203404.
[32] Q. Zeng, S. Wan, S. Yang, X. Zhao, F. He, Y. Zhang, X. Cao, Q. Wen, Y. Feng, G. Yu, Super stretchability, strong adhesion, flexible sensor based on Fe3+ dynamic coordination sodium alginate/polyacrylamide dual-network hydrogel, Colloids Surfaces A Physicochem. Eng. Asp. 652 (2022), 129733.
[33] G. Huang, Z. Tang, S. Peng, P. Zhang, T. Sun, W. Wei, L. Zeng, H. Guo, H. Guo, G. Meng, Modification of hydrophobic hydrogels into a strongly adhesive and tough hydrogel by electrostatic interaction, Macromolecules 55 (2021) 156–165.
[34] D.M. Ibrahim, E.S. Sani, A.M. Soliman, N. Zandi, E. Mostafavi, A.M. Youssef, N. K. Allam, N. Annabi, Bioactive and elastic nanocomposites with antimicrobial properties for bone tissue regeneration, ACS Appl. Bio Mater. 3 (2020) 3313–3325.
[35] Y. Wang, H. Wu, Z. Wang, J. Zhang, J. Zhu, Y. Ma, Z. Yang, Y. Yuan, Optimized synthesis of biodegradable elastomer pegylated poly (glycerol sebacate) and their biomedical application, Polymers 11 (2019) 965.
[36] Y. Wu, L. Wang, B. Guo, P.X. Ma, Injectable biodegradable hydrogels and microgels based on methacrylated poly (ethylene glycol)-co-poly (glycerol sebacate) multi-block copolymers: synthesis, characterization, and cell encapsulation, J. Mater. Chem. B 2 (2014) 3674–3685.
[37] Y. Ma, W. Zhang, Z. Wang, Z. Wang, Q. Xie, H. Niu, H. Guo, Y. Yuan, C. Liu, PEGylated poly (glycerol sebacate)-modified calcium phosphate scaffolds with desirable mechanical behavior and enhanced osteogenic capacity, Acta Biomater. 44 (2016) 110–124.
[38] S.M. Davachi, S.M.A. Haramshahi, S.A. Akhavirad, N. Bahrami, S. Hassanzadeh, S. Ezzatpour, N. Hassanzadeh, M.M. Kebria, M. Khanmohammadi, Z. Bagher, Development of chitosan/hyaluronic acid hydrogel scaffolds via enzymatic reaction for cartilage tissue engineering, Mater. Today Commun. 30 (2022), 103230.
[39] K. Yang, J. Zhang, X. Ma, Y. Ma, C. Kan, H. Ma, Y. Li, Y. Yuan, C. Liu, β-Tricalcium phosphate/poly (glycerol sebacate) scaffolds with robust mechanical property for bone tissue engineering, Mater. Sci. Eng. C 56 (2015) 37–47.
[40] J.P. Mofokeng, A.S. Luyt, Morphology and thermal degradation studies of melt-mixed poly (lactic acid)(PLA)/poly (ε-caprolactone)(PCL) biodegradable polymer blend nanocomposites with TiO2 as filler, Polym. Test. 45 (2015) 93–100.
[41] S. Wang, M.J. Yaszemski, J.A. Gruetzmacher, L. Lu, Photo-crosslinked poly (ϵ-caprolactone fumarate) networks: roles of crystallinity and crosslinking density in determining mechanical properties, Polymer 49 (2008) 5692–5699.
[42] C.C. Lau, M. Al Qaysi, N. Owji, M.K. Bayazit, J. Xie, J.C. Knowles, J. Tang, Advanced biocomposites of poly (glycerol sebacate) and β-tricalcium phosphate by in situ microwave synthesis for bioapplication, Mater, Today Adv 5 (2020), 100023.
[43] A. Patel, A.K. Gaharwar, G. Iviglia, H. Zhang, S. Mukundan, S.M. Mihaila, D. Demarchi, A. Khademhosseini, Highly elastomeric poly (glycerol sebacate)-co-poly (ethylene glycol) amphiphilic block copolymers, Biomaterials 34 (2013) 3970–3983.
[44] R. Najafi, H. Chahsetareh, M. Pezeshki-Modaress, M. Aleemardani, S. Simorgh, S. M. Davachi, R. Alizadeh, A. Asghari, S. Hassanzadeh, Z. Bagher, Alginate sulfate/ECM composite hydrogel containing electrospun nanofiber with encapsulated human adipose-derived stem cells for cartilage tissue engineering, Int. J. Biol. Macromol. (2023), 124098.
[45] S.S. Garakani, S.M. Davachi, Z. Bagher, A.H. Esfahani, N. Jenabi, Z. Atoufi, M. Khanmohammadi, A. Abbaspourrad, H. Rashedi, M. Jalessi, Fabrication of chitosan/polyvinylpyrrolidone hydrogel scaffolds containing PLGA microparticles loaded with dexamethasone for biomedical applications, Int. J. Biol. Macromol. 164 (2020) 356–370.
[46] S. Yoon, B. Chen, Elastomeric and pH-responsive hydrogels based on direct crosslinking of the poly (glycerol sebacate) pre-polymer and gelatin, Polym. Chem. 9 (2018) 3727–3740.
[47] S.M. Ali, G. Yosipovitch, Skin pH: from basic science to basic skin care, Acta Derm. Venereol. 93 (2013) 261–269.
[48] M.T. Ghoneim, A. Nguyen, N. Dereje, J. Huang, G.C. Moore, P.J. Murzynowski, C. Dagdeviren, Recent progress in electrochemical pH-sensing materials and configurations for biomedical applications, Chem. Rev. 119 (2019) 5248–5297.
[49] L. Xu, L. Qiu, Y. Sheng, Y. Sun, L. Deng, X. Li, M. Bradley, R. Zhang, Biodegradable pH-responsive hydrogels for controlled dual-drug release, J. Mater. Chem. B 6 (2018) 510–517.
[50] W. Wu, J. Liu, S. Cao, H. Tan, J. Li, F. Xu, X. Zhang, Drug release behaviors of a pH sensitive semi-interpenetrating polymer network hydrogel composed of poly (vinyl alcohol) and star poly [2-(dimethylamino) ethyl methacrylate], Int. J. Pharm. 416 (2011) 104–109.
[51] O. Cevik, D. Gidon, S. Kizilel, Visible-light-induced synthesis of pH-responsive composite hydrogels for controlled delivery of the anticonvulsant drug pregabalin, Acta Biomater. 11 (2015) 151–161.
[52] C. Chang, Y. Yeh, Poly (glycerol sebacate)-co-poly (ethylene glycol)/gelatin hybrid hydrogels as biocompatible biomaterials for cell proliferation and spreading, Macromol. Biosci. (2021), 2100248.
[53] M. Rahmati, J.J. Blaker, S.P. Lyngstadaas, J.F. Mano, H.J. Haugen, Designing multigradient biomaterials for skin regeneration, Mater, Today Adv 5 (2020), 100051.
[54] S. Nour, R. Imani, M. Mehrabani, A. Solouk, M. Iranpour, S. Jalili-Firoozinezhad, A. M. Sharifi, Biomimetic hybrid scaffold containing niosomal deferoxamine promotes angiogenesis in full-thickness wounds, Mater, Today Chem 27 (2023), 101314.
[55] M. Aleemardani, M.Z.Z. Trikić, N.H.H. Green, F. Claeyssens, The importance of mimicking dermal-epidermal junction for skin tissue engineering: a review, Bioengineering 8 (2021) 148.
[56] M. Aleemardani, A. Solouk, S. Akbari, M.M. Dehghan, M. Moeini, Silk-derived Oxygen-Generating Electrospun Patches for Enhancing Tissue Regeneration: Investigation of Calcium Peroxide Role and its Effects in Controlled Oxygen Delivery, Materialia, 2020, 100877.
[57] E.S. Sani, A. Kheirkhah, D. Rana, Z. Sun, W. Foulsham, A. Sheikhi, A. Khademhosseini, R. Dana, N. Annabi, Sutureless repair of corneal injuries using naturally derived bioadhesive hydrogels, Sci. Adv. 5 (2019), eaav1281.
[58] B. Saleh, H.K. Dhaliwal, R. Portillo-Lara, E. Shirzaei Sani, R. Abdi, M.M. Amiji, N. Annabi, Local immunomodulation using an adhesive hydrogel loaded with miRNA-laden nanoparticles promotes wound healing, Small 15 (2019), 1902232.
[59] A. Pizzi, K.L. Mittal, Handbook of Adhesive Technology, CRC Press, 2017.
[60] H. Montazerian, E. Davoodi, A.H. Najafabadi, R. Haghniaz, A. Baidya, N. Annabi, A. Khademhosseini, P.S. Weiss, Injectable gelatin-oligo-catechol conjugates for tough thermosensitive bioadhesion, Cell Reports Phys. Sci. 4 (2023).
[61] V. Krishnadoss, B. Kanjilal, A. Masoumi, A. Banerjee, I. Dehzangi, A. Pezhouman, R. Ardehali, M. Martins-Green, J. Leijten, I. Noshadi, Programmable bio-ionic liquid functionalized hydrogels for in situ 3D bioprinting of electronics at the tissue interface, Mater, Today Adv 17 (2023), 100352.
[62] J. Li, X. Yu, E.E. Martinez, J. Zhu, T. Wang, S. Shi, S.R. Shin, S. Hassan, C. Guo, Emerging Biopolymer-Based Bioadhesives, Macromol. Biosci., 2021, 2100340.
[63] W.D. Spotnitz, Fibrin sealant: the only approved hemostat, sealant, and adhesive—a laboratory and clinical perspective, Int. Sch. Res. Notices 2014 (2014).
[64] A. Baidya, M. Ghovvati, C. Lu, H. Naghsh-Nilchi, N. Annabi, Designing a nitro-induced sutured biomacromolecule to engineer electroconductive adhesive hydrogels, ACS Appl. Mater. Interfaces 14 (2022) 49483–49494.
[65] S. Moazami, M. Kharaziha, R. Emadi, M. Dinari, Multifunctional bioinspired bredigite-modified adhesive for bone fracture healing, ACS Appl. Mater. Interfaces 15 (2023) 513–6499.
[66] E. Shirzaei Sani, R. Portillo-Lara, A. Spencer, W. Yu, B.M. Geilich, I. Noshadi, T. J. Webster, N. Annabi, Engineering adhesive and antimicrobial hyaluronic acid/elastin-like polypeptide hybrid hydrogels for tissue engineering applications, ACS Biomater. Sci. Eng. 4 (2018) 2528–2540.
[67] A. Faghihnejad, K.E. Feldman, J. Yu, M. V Tirrell, J.N. Israelachvili, C.J. Hawker, E. J. Kramer, H. Zeng, Adhesion and surface interactions of a self-healing polymer with multiple hydrogen-bonding groups, Adv. Funct. Mater. 24 (2014) 2322–2333.
[68] X. Zou, X. Wang, M. Gou, O. Yue, Z. Bai, H. Zhang, X. Liu, Ultra-strong adhesive, self-healing and electroactive bio-based hydrogels for the on-demand fabrication of sandwich-inspired smart electronic sensing floors, J. Mater. Chem. A. 10 (2022) 14555–14567.

[69] H. Guo, C. Zhu, Z. Yuan, G. Huang, H. Liang, C. Xiong, Z. Feng, Q. Wei, G. Meng, Facile hydrogels of AIEgens applied as reusable sensors for in situ and early warning of metallic corrosion, ACS Appl. Mater. Interfaces 15 (2023) 8530–8536.
[70] M.-B. Yi, T.-H. Lee, S.-J. Lee, J.-S. Kim, H.-J. Kim, Topologically designed cross-linking network for stretchable and recoverable pressure-sensitive adhesives with exceptional softness, Mater. Today Chem. 26 (2022), 101141.
[71] Z. Xiao, Q. Li, H. Liu, Q. Zhao, Y. Niu, D. Zhao, Adhesion mechanism and application progress of hydrogels, Eur. Polym. J. (2022), 111277.
[72] S. Huang, D. Lei, Q. Yang, Y. Yang, C. Jiang, H. Shi, B. Qian, Q. Long, W. Chen, Y. Chen, A perfusable, multifunctional epicardial device improves cardiac function and tissue repair, Nat. Med. 27 (2021) 480–490.
[73] S. Rastegar, M. Mehdikhani, A. Bigham, E. Poorazizi, M. Rafienia, Poly glycerol sebacate/polycaprolactone/carbon quantum dots fibrous scaffold as a multifunctional platform for cardiac tissue engineering, Mater. Chem. Phys. 266 (2021), 124543.
[74] S. Dikici, F. Claeyssens, S. MacNeil, Decellularised baby spinach leaves and their potential use in tissue engineering applications: studying and promoting neovascularisation, J. Biomater. Appl. 34 (2019) 546–559.
[75] I. Colombo, E. Sangiovanni, R. Maggio, C. Mattozzi, S. Zava, Y. Corbett, M. Fumagalli, C. Carlino, P.A. Corsetto, D. Scaccabarozzi, HaCaT cells as a reliable in vitro differentiation model to dissect the inflammatory/repair response of human keratinocytes, Mediat. Inflamm. (2017) (2017).
[76] M. Farokhi, M. Aleemardani, A. Solouk, H. Mirzadeh, A.H. Teuschl, H. Redl, Crosslinking strategies for silk fibroin hydrogels: promising biomedical materials, Biomed. Mater. 16 (2021), 22004, https://doi.org/10.1088/1748-605x/abb615.
[77] A. Randhawa, S.D. Dutta, K. Ganguly, D.K. Patel, T. V Patil, K. Lim, Recent advances in 3D printing of photocurable polymers: types, mechanism, and tissue engineering application, Macromol. Biosci. 23 (2023), 2200278.